

Electronic Supplementary Material (ESI) for Faraday Discussions.

This journal is © The Royal Society of Chemistry 2017

## Supporting Material

### Large-scale QM/MM calculations of the $\text{CaMn}_4\text{O}_5$ cluster in the $\text{S}_3$ state of the oxygen evolving complex of photosystem II. Comparisons between water-inserted and no water-inserted structures

Mitsuo Shoji<sup>a,b,\*</sup>, Hiroshi Isobe<sup>c</sup>, Takahito Nakajima<sup>d</sup>, Yasuteru Shigeta<sup>a</sup>, Michihiro Suga<sup>c</sup>, Fusamichi Akita<sup>c</sup>, Jian-Ren Shen<sup>c</sup>, Kizashi Yamaguchi<sup>d,e,f,\*</sup>

<sup>a</sup> Center for Computational Sciences, University of Tsukuba, Tennodai 1-1-1, Tsukuba, Ibaraki 305-8577, Japan

<sup>b</sup> Graduate School of Pure and Applied Sciences, University of Tsukuba, Tennodai 1-1-1, Tsukuba, Ibaraki 305-8577, Japan

<sup>c</sup> Photosynthesis Research Center, Graduate School of Natural Science and Technology, Faculty of Science, Okayama University, Okayama, Okayama 700-8530, Japan

<sup>d</sup> Riken Advanced Institute for Computational Science, Kobe, Hyogo 650-0047, Japan

<sup>e</sup> Institute for NanoScience Design, Osaka University, Toyonaka, Osaka 560-8531, Japan

<sup>f</sup> Handairigaku Techno-Research (NPO), Toyonaka, Osaka 560-0043, Japan.

After the submission of this paper two important papers concerning with the  $\text{S}_3$  state of OEC of PSII were published. Berkeley group has reported the  $\text{S}_3$  (two flash irradiation) structure of OEC of PSII by serial femtosecond X-ray diffraction (SFX) method (I. Young et al., Nature 540, 453-457 (2016)), concluding no insertion of hydroxide anion in the  $\text{S}_1$  to  $\text{S}_3$  transition. Very recently, Okayama group has shown the SFX difference map responsible for the insertion of water molecule in the  $\text{S}_1$  to  $\text{S}_3$  transition (Suga et al, Nature 543, 131-135 (2017)). Thus key conclusions on the  $\text{S}_3$  structure of OEC of PSII are different between Berkeley and Okayama groups. In the Faraday discussion on artificial photosynthesis (AP) at Kyoto (2017) extensive discussions have been performed for understanding possible origins of different conclusions reported by Berkeley and Okayama groups. However, we could not explain our theoretical views for questions (partly because of the time limit for presentation) concerning with the O-O bond formation for water oxidation in relation to the latest finding. In this supporting material several figures (Figs. S13-S22) used in the discussion session are included for theoretical understanding of the mechanism of water oxidation in OEC of PSII.

In this supporting material our large-scale QM/MM models are briefly described concerning with the questions 201-203 in Faraday Discussions in the supporting section SI. Full optimized geometries and

electronic structures of several possible intermediates in the  $S_3$  state are shown in the section SII. Theoretical backgrounds for understanding the metal diradical character ( $\cdot M-O \cdot$ ) of the high-valent transition-metal oxo bonds ( $Mn=O_{(4)}$ ,  $Mn=O_{(5)}$ ) are summarized for understanding (question No. 200) of the radical coupling mechanisms of the O-O bond formation (question No. 203) in water oxidation in native and artificial photosynthesis in the section SIII. Concerning with the questions 201 and 202, future prospects of theoretical investigation are given in the section SIV.

## SI Large scale QM/MM modeling of OEC of PSII

### SI. 1 Theoretical modeling of the $CaMn_4O_5$ cluster in OEC of PSII

Our fundamental concept for theoretical modeling is that OEC of PSII is a typical biomolecular system consisted of several parts such as the  $CaMn_4O_5$  catalyst, several channels for proton transfer, water inlet, light-harvesting antenna, etc. We have already examined the system structure of OEC of PSII in one chapter of the book (see ref. 10), emphasizing the necessity of appropriate QM/MM models for theoretical investigation of several biological functions of OEC of PSII under consideration. In order to elucidate possible mechanisms of the water oxidation in OEC of PSII, a large-scale QM/MM model<sup>10,11</sup> has been constructed based on the basis of the XRD structure<sup>3</sup> of the OEC of PSII at 1.9 Å resolution as shown in Fig. S1. Minimal QM model (Min1) in the present theoretical modeling involves ten amino acid residues coordinated to the  $CaMn_4O_5(H_2O)_4$  core: Ser169, Asp170, Glu189, His190, Asp342-Leu343-Ala344, His332-Glu333 and Glu354 as shown in Fig. S1A. In addition to the Min1 model, Asp61, His337, Asn338 and Arg357, together with 14 water molecules, have been considered in an intermediate QM (Min2) model in Fig. S1B. Full QM model in this modeling further involves Tyr161, Glu165, Asn181, Phe182, Val185, Asn298, Lys317, Cl679(Cl<sub>1</sub>) and Cl680(Cl<sub>2</sub>) as shown in Fig. S1C. Inclusion of Val185 and Lys317 into the QM part is essential for understanding of recent mutational experiments<sup>49</sup>. We here consider explicitly 27 extra water molecules ( $H_2O_{(i)}$ ) in the last model around the  $CaMn_4O_5(H_2O)_4$  core in the coordination sphere elucidated by SP8 XRD<sup>3</sup>.

The high-resolution XRD<sup>3</sup> structure revealed the charge balances in the  $S_1$  state of OEC of PSII<sup>33</sup>:  $\{His337^+, Cl_2^-\}$ ,  $\{Arg357^+, Asp61^-\}$ ,  $\{Lys317^+, Cl_1^-\}$ , and  $\{Arg334^+, Glu312^-\}$  around the  $CaMn_4O_5$  cluster. Therefore its charge neutralization structure in the  $S_1$  state was found to be  $Ca(II)Mn(III)_2Mn(IV)_2O_5(H_2O)_4$  ( $X=O^{2-}$ ,  $Y=Z=H_2O$ ,  $W=null$ ) in our early paper (see Fig. 2 in the text)<sup>32,33</sup>. However, other theoretical groups assumed different structures. For example, structures including  $\{Lys317^+, Cl_1^-\}$  and  $\{His337^+, null\}$  requires the deprotonation of Y ( $Y=OH^-$ ) for charge neutralization in the  $S_1$  state<sup>19-29</sup>. As shown in the text, different starting trial geometries provided different optimized structures that were compared with EXAFS results<sup>5-7</sup> as summarized in Table 3.

As shown in Fig. 2, the  $Ca(II)Mn(III)_2Mn(IV)_2O_5(H_2O)_4$  ( $X=O^{2-}$ ,  $Y=Z=H_2O$ ,  $W=null$ ) can be transformed into a geometrical isomer,  $Ca(II)Mn(III)_2Mn(IV)_2O_5(H_2O)_4$  ( $X=Y=OH^-$ ,  $Z=H_2O$ ,  $W=null$ ). Relative stabilities between these isomers might be variable, depending on packing modes of crystals of PSII, types of crystallization materials employed, structures of hydrogen-bonding networks, pH, etc. since

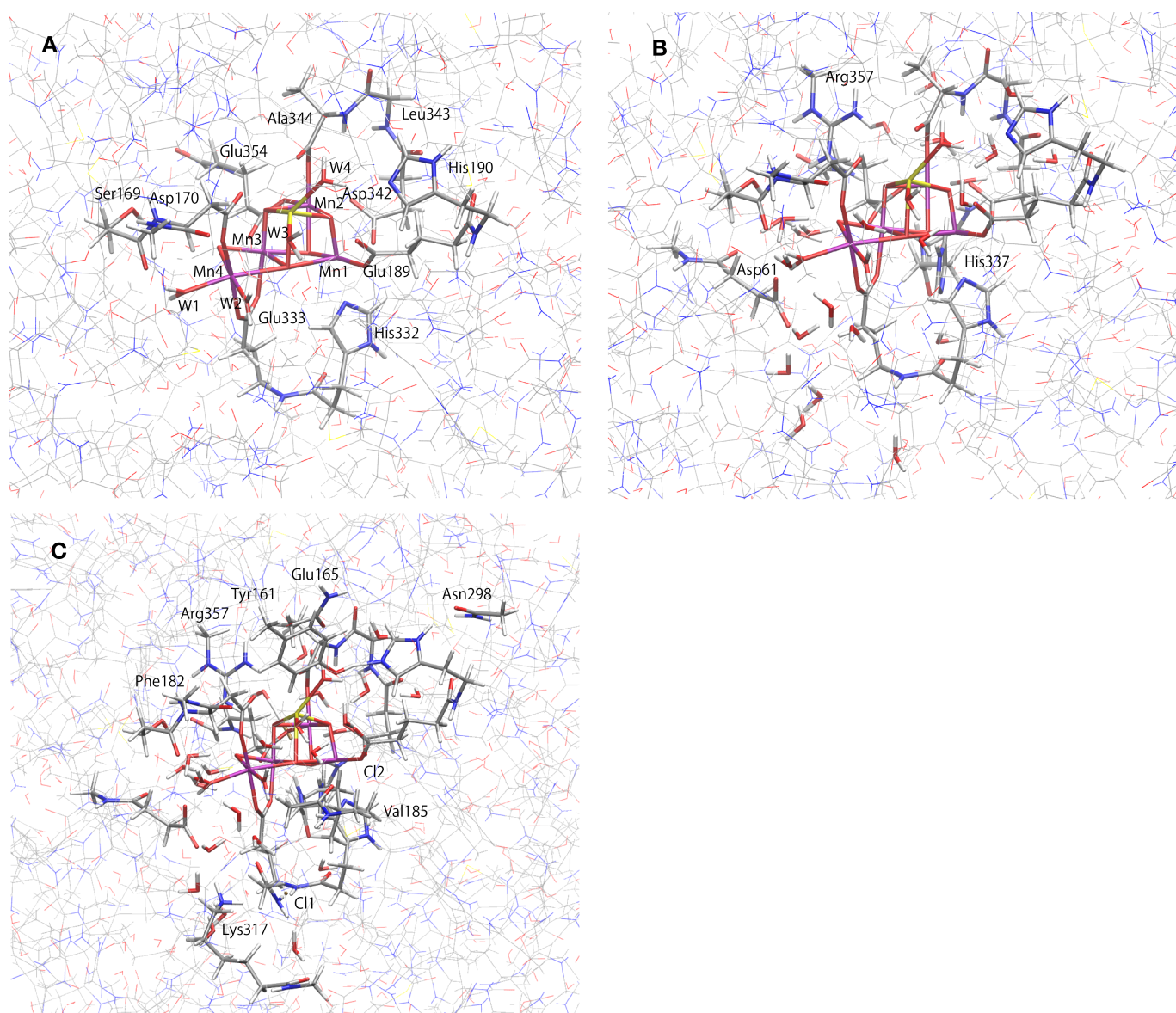


Fig. S1 QM/MM models used in this study. (A) Min1: minimal atoms are included in the QM region, (B) Min2: atoms of water atoms and charged amino acid residues are added to the Min1 model (C) Full: all the atoms near the OEC active site are included.

the chemical bonds of the  $\text{CaMn}_4\text{O}_5$  cluster are labile<sup>32</sup> because of the Jahn-Teller effect of the Mn(III) ion. Careful examination and understanding of experimental conditions are crucial for theoretical modeling of complex biomolecular systems such as OEC of PSII. X-ray damage free XRD structure with higher resolution than 1.9 Å (for example 1.5 Å) is also desirable for precise theoretical modeling.

In order to reduce the computational complexity, Asp342-Leu343-Ala344 ligand for the QM part is simply modeled as the loop:  $-\text{O}-\text{C}(=\text{O})-\text{CH}_2-\text{CH}_2-\text{CH}_2-\text{CO}-\text{NH}-\text{CO}-\text{NH}-\text{CH}_2-\text{CO}-\text{NH}-\text{CH}(\text{CH}_3)-\text{COO}-$  (see Fig. S1A). Similarly Glu333-His332 ligand for QM is approximated by the loop:  $-\text{OOC}-\text{CH}_2-\text{CH}_2-\text{NH}-\text{CO}-\text{NH}-\text{CH}_2-\text{CH}_2-\text{methyl imidazole}$ . His337-Asn338 ligands are modeled by methyl

imidazole-CO-NH-CH<sub>2</sub>-C(C=O)-NH<sub>2</sub> to elucidate the hydrogen bonding networks. These amino acid residues confine the CaMn<sub>4</sub>O<sub>5</sub> core in OEC of PSII, where a more realistic confined model revealed by the XRD is illustrated in Fig. S1. In this paper the remaining backbone aminoacid chains in Fig. S1 are considered using the molecular mechanics (MM) model for taking into account for the confinement effect. Details are given in ref. 10. The large-scale QM/MM models are re-visited in relation to the questions 201-203 in Faraday Discussions in section IV, namely future prospect.

## SI. 2 Kok cycle for water oxidation

The Kok cycle<sup>1,2</sup> for water oxidation in OEC of PSII is illustrated in Fig. S2. Insertion of a water molecule at the S<sub>2</sub> to S<sub>3</sub> transition was not assumed in Fig. S2. Therefore two water molecules will be inserted at the S<sub>3</sub>-S<sub>4</sub>-S<sub>0</sub> transition. Large QM/MM calculations have elucidated that the S<sub>3</sub> state with the (4444) valence configuration is feasible under the assumption of double deprotonations of W1 and W2 (W1=W2=OH<sup>-</sup>) of the CaMn<sub>4</sub>O<sub>5</sub> cluster as discussed in details in the text. The experimental result by Berkeley group (I. Young et al., Nature 540, 453-457 (2016)) is consistent with the Kok cycle in Fig. S2. On the other hand, the insertion of a water molecule at the S<sub>2</sub> to S<sub>3</sub> transition is the other possibility that has been assumed in our other papers.<sup>10</sup> The experimental result by Okayama group (Suga et al, Nature 543, 131-135 (2017)) is consistent with the other Koc cycle given in the ref. 10. The contents in the text are therefore timely and suggestive for understanding of the experimental results by both groups.

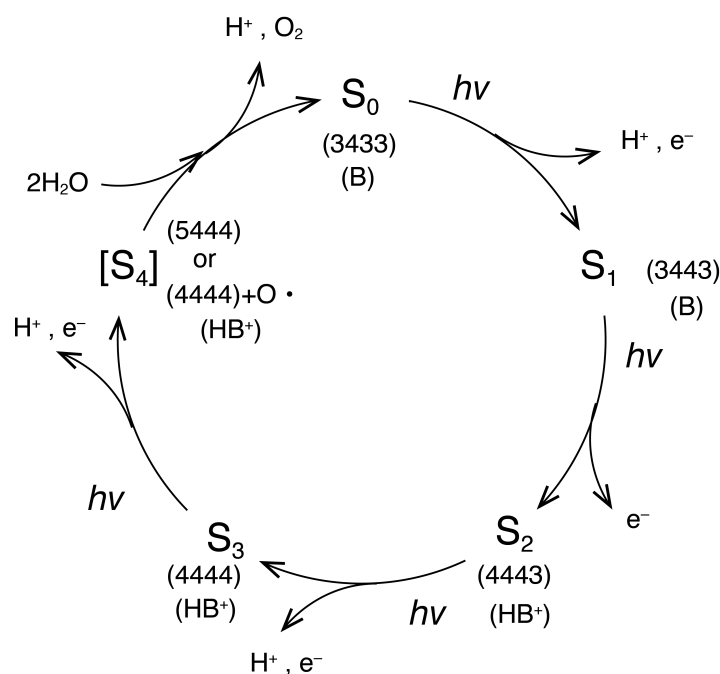


Fig. S2 The Kok cycle for water oxidation in OEC of PSII. No water insertion was assumed in the S<sub>2</sub> to S<sub>3</sub> transition. The trapping of proton with base (B) was assumed for no release of proton in the S<sub>1</sub> to S<sub>2</sub> transition for deprotonation of W2 (W2=OH<sup>-</sup>).

## SII Possible mechanisms for the O-O bond formation

### SII. 1 Molecular orbital (FMO) model for prediction of reaction sites for water oxidation

The oxygen dianion sites  $O_{(5)}$  and  $O_{(4)}$  in the  $CaMn_4O_5$  cluster in OEC of PSII play important roles for water oxidation as illustrated in Figs. S3-S9. This is a reply for the questions 200 and 203 concerning with possible roles of these sites. Frontier molecular orbital (FMO) analysis<sup>38</sup> was a our first theoretical step for elucidation of intrinsic property of chemical bonds of the  $CaMn_4O_5$  cluster in OEC of PSII after the discovery of the high-resolution XRD structure.<sup>3</sup> To this end, FMO analysis was performed for possible valence states of the  $CaMn_4O_5$  cluster in the  $S_0$ - $S_4$  states assuming the XRD structure.<sup>3</sup> The HOMO and LUMO of the  $CaMn_4O_5$  cluster in the formal (4444) oxidation state clearly indicated three possible intrinsic reaction sites, namely  $O_{(5)}$ ,  $O_{(4)}$  and W2 sites. Thus the reaction pathways (A)-(D) in Scheme I<sup>17</sup> in the text were proposed on the basis of the FMO theory<sup>38</sup> for which the LUMO of the  $CaMn_4O_5$  cluster in the  $S_3$  (or  $S_3$  plus tyr-radical in the early  $S_4$  state) state under the assumption of the XRD structure<sup>3</sup> played significant role for prediction of the reaction sites.

As a next step, we must consider much more faithful theoretical models for OEC of PSII revealed by XRD<sup>3</sup> and XFEL<sup>4</sup> to elucidate possible reaction pathways (A)-(D) for water oxidation. XRD<sup>3</sup> and XFEL<sup>4</sup> experiments have revealed the  $S_1$  structure of the  $CaMn_4O_5$  cluster and channel structures around the cluster. However, high-resolution XRD and XFEL results were lacking for the  $S_3$  state even several months ago. Therefore we did not have clear-cut answer for water insertion step in the Kok cycle on the experimental grounds. Nowadays Berkeley and Okayama groups have reported the  $S_3$  structures by SFX and XFEL techniques. However, current situations for water insertion in the  $S_2$  to  $S_3$  transition were different between these leading groups. Thus the  $S_3$  structures by SFX are not conclusive yet. Nevertheless the SFX results by both groups indicated the participations of the  $O_{(5)}$  site for water oxidation, supporting the FMO analysis.<sup>38</sup>

### SII. 2 Possible reaction pathways for formation of Mn-O-OH and related species

It may be advisable to consider both cases at the moment, namely

- (i) insertion of water in the  $S_2$  to  $S_3$  transition, and
- (ii) no insertion of water in the  $S_2$  to  $S_3$  transition,

on the theoretical grounds. Possible reaction pathways under the assumption of (i) have been extensively investigated on the basis of hybrid density functional (HDFT) methods as discussed in the text.<sup>10, 15</sup> However relative stabilities of several key intermediates in the  $S_3$  state are highly dependent on the HDFT functionals, particularly fraction of the Hartree-Fock component, employed as shown in our recent papers<sup>14, 15</sup>. This is a characteristic feature of the strongly correlated electron systems (SCES) in general (see also Table S1). Therefore careful examinations of HDFT results by post HDFT calculations such as the density matrix renormalized group (DMRG)<sup>71, 72</sup> are inevitable for quantitative discussions on the reaction pathways even in the case of (i).

Theoretical investigations of possible reaction pathways in the case of (ii) are rather limited. Figs.

S3-S5 illustrates possible reactions pathways in Scheme I (see text) under the assumption of no water insertion in the  $S_2$  to  $S_3$  transition. An important feature in the case of (ii) is that the O-OH coupling becomes feasible with participation of hydrogen bonding networks that are often neglected in small-scale QM models. Water-assisted mechanisms for the O-OH bond formation of water oxidation<sup>36-38</sup> are not at all trivial for OEC of PSII even now because unexpected structural changes in the  $S_3$ - $S_4$  transition are not excluded yet. The following pathways are given as

(Fig. S3) Possible A-like pathway in Scheme I, namely attack of W3 to the  $O_{(5)}$  site,

(Fig. S4) Possible B-like pathway in Scheme I, namely attack of W2(=OH-) to the  $O_{(5)}$  site

(Fig. S5) Possible C-like pathway in Scheme I, namely attack of W11 to the  $O_{(4)}$  site.

In the text, we did not touch possibility of formation of the  $Mn_{a(4)}-O_{(5)}-O_{(6)}-H$  even in the  $S_3$  state in relation to the XFEL result by Suga et al. (Nature 543, 131-135 (2017)). In fact, the  $O_{(5)}-O_{(6)}$  distance of the Mn-O-OH is about 1.45 Å in consistent with the experimental value by XFEL. Moreover the short  $O_{(6)}-O(\text{Glu189})$  distance (2.6 Å) by XFEL is also consistent with the strong hydrogen bonding. Formation of Mn-O-OH may be feasible under the assumption of formation of the photo-induced non-equilibrium state in the  $S_3$  state, in accord with the Renger mechanism<sup>61</sup> (Journal of Photochemistry and Photobiology B; Biology, 104, 35 (2011)). However, at the moment there is no spectroscopic result for formation of the O-OH bond in the  $S_3$  state. Moreover the XES spectroscopy indicated that the valence state of the  $CaMn_4$  cluster can be regarded as  $Ca(II)Mn(IV)_4$  in the  $S_3$  state in contradiction to that of the hydroperoxide (see Fig. S19). Alternately, the  $S_3 + \text{tyr-O} \cdot$  state after the third flash may be considered as a precursor for the OO bond formation in the path A; the same is true for the paths B and C. Scheme I is applicable for the above both cases.

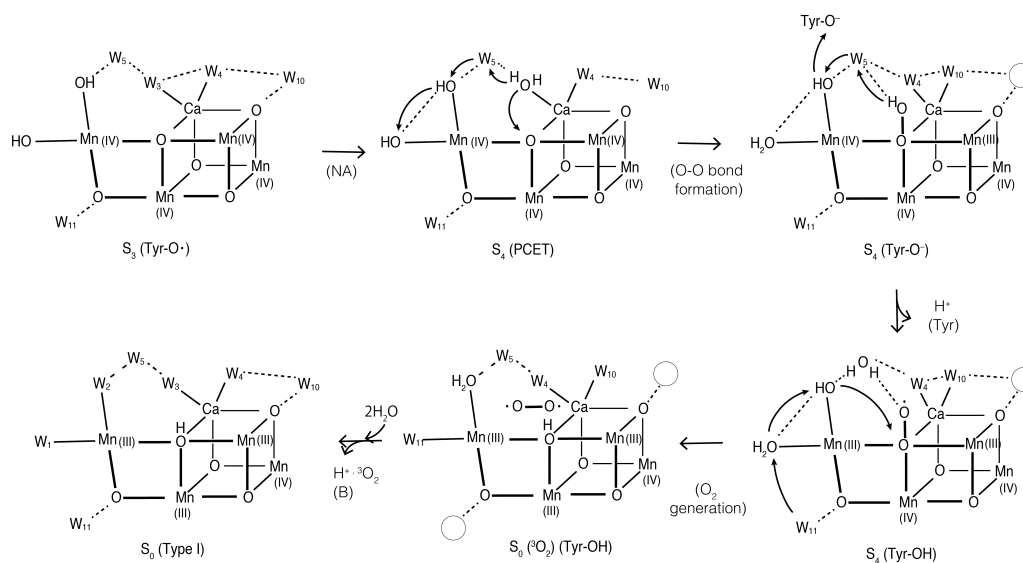


Fig. S3 Possible A-like pathway in Scheme I for the O-OH coupling for water oxidation in OEC of PSII<sup>17</sup>. W3 attacks the  $O_{(5)}$  site for the OO bond formation.

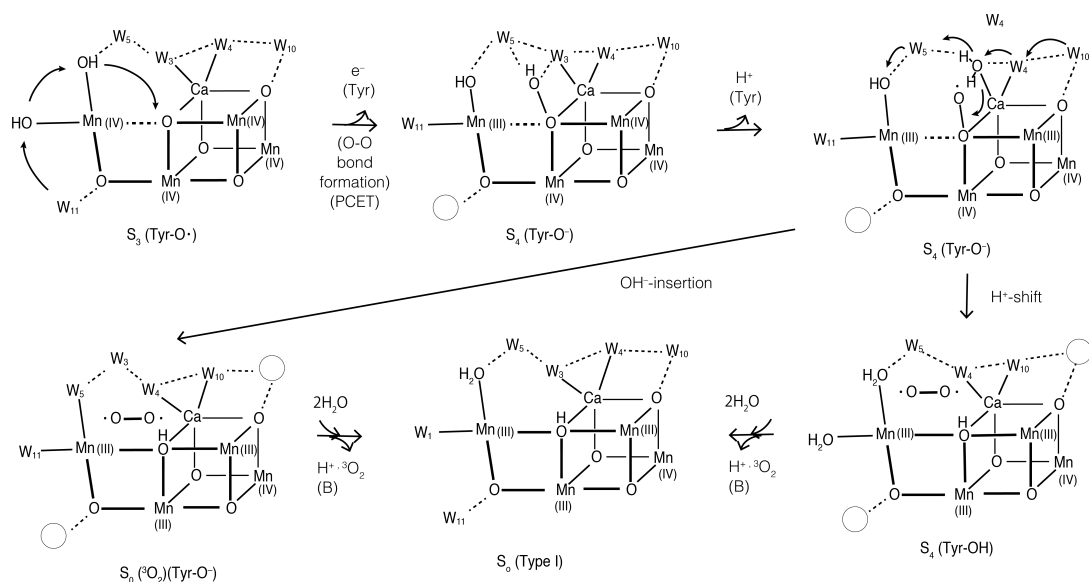


Fig. S4 Possible B-like pathway in Scheme I for the O-OH coupling for water oxidation in OEC of PSII<sup>17</sup>. W2(=OH-) attacks the O<sub>(5)</sub> site for the OO bond formation in this model.

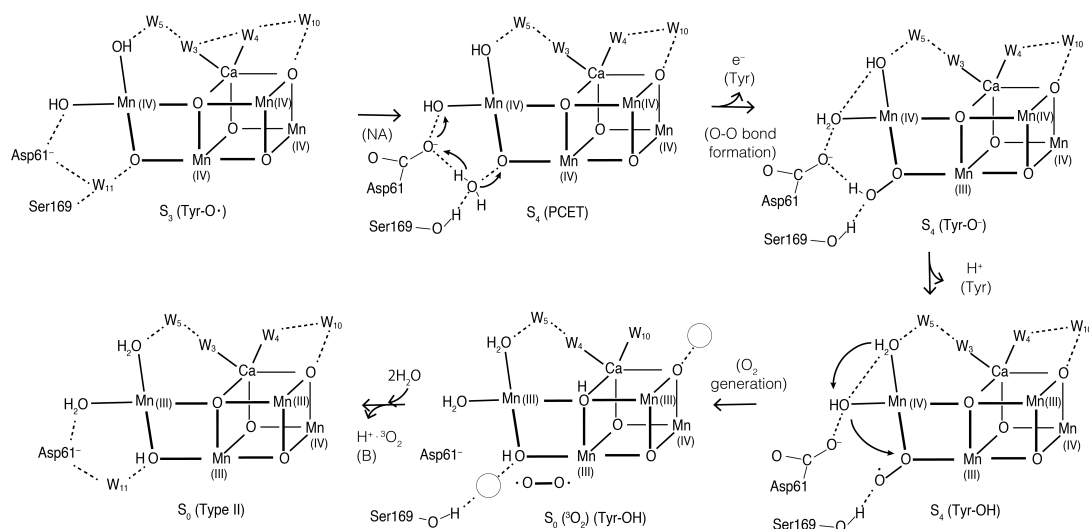


Fig. S5 Possible C-like pathway in Scheme I for the O-OH coupling for water oxidation in OEC of PSII<sup>17</sup>. W11(=OH-) attacks the O<sub>(4)</sub> site for the OO bond formation in this model.

### SII. 3 Metal diradical character for high-valent transition-metal oxo bonds

The nature of the high-valent transition-metal oxo bonds (M=O) is closely related to possible roles of the O<sub>(5)</sub> and O<sub>(4)</sub> sites, namely Mn=O<sub>(5)</sub> and Mn=O<sub>(4)</sub>, of the CaMn<sub>4</sub>O<sub>5</sub> cluster in OEC of PSII, (reply to the question 200). The transition-metal oxo (MO) bonds are usually regarded as M<sup>2+</sup>O<sup>2-</sup>, indicating that the oxygen site is oxygen dianion (O<sup>2-</sup>) responsible for the nucleophilic reactivity. In early 1980<sup>th</sup> the high-valent transition-metal oxo bonds were found to exhibit the radical or electrophilic reactivity. Discovery of the unexpected reactivity was a topic at the Hawaii pacific chem. conference in 1984.

Therefore we have extended broken-symmetry (BS) MO theoretical calculations of transition-metal oxo species  $M=O$  ( $M=Ti, V, Cr, Mn, Fe, Ni, Cu$ ) to elucidate the nature of  $d\sigma-p\sigma$  and  $d\pi-p\pi$  bonds<sup>43</sup>. Early transition-metal oxo bonds were found to be metal zwitterions (ZW), namely  $[Ti(IV)O^2]^{2+}$  and  $[V(IV)O^2]^{2+}$ . Therefore the oxygen site of these species was responsible for the nucleophilic reactivity. The BS computations indicated that the photo-induced charge-transfer (CT) from  $O^{2-}$  to early transition metals such as  $Ti(IV)$ ,  $V(V)$  was necessary for generation of the  $\bullet Ti(III)-O\bullet$  or  $\bullet V(IV)-O\bullet$  bond that has active oxygen for electrophilic or radical reactivity.



The oxyl radical character generated by photo-excitation is considered to be responsible for the photo-catalytic oxidation in several artificial systems.

Early molecular orbital (MO) calculations<sup>43</sup> have revealed that the high-valent  $M=O$  species such as  $[Mn(IV)=O]^{2+}$  and  $[Fe(IV)=O]^{2+}$  exhibit electrophilic property in a sharp contrast with nucleophilic character expected for low-valent  $M=O$  bonds:  $[M(m)O^2]^{m-2}$ . However, as mentioned above, the origin of diradical character of the high-valent metal-oxo bonds was the mystery in early 1980<sup>th</sup>. The broken-symmetry (BS) calculations<sup>43</sup> have opened a new era of the MO theory of such labile chemical bonds, namely “orbital symmetry breaking” in contrast to the orbital symmetry conservation. Indeed, the BS methods have elucidated that the closed-shell  $d\pi-p\pi$  bonds of high-valent  $M=O$  species often suffer the triplet-instability, giving rise to open-shell (BS) configurations with significant metal-diradical (MDR) character  $\bullet M-O\bullet$  as shown in Fig. S6. The local spins ( $\bullet$ ) generated by the orbital symmetry breaking are often described by the Heisenberg spin Hamiltonian models<sup>32</sup> as shown below.

One of the key concepts in broken-symmetry (BS) approach to strongly correlation electron system (SCES) is indeed the HOMO-LUMO mixing<sup>43</sup> as illustrated in Fig. S6. As an example, let us consider the  $d\pi-p\pi$  bond of transition-metal oxo ( $M=O$ ) species. The HOMO exhibits the in-phase orbital symmetry responsible for the covalent bonding between metal and oxygen atoms. On the other hand, the LUMO exhibits the out of phase orbital symmetry responsible for the antibonding character between metal and oxygen atoms. The HOMO-LUMO gap for stable  $M=O$  bond is usually large, indicating that the up- and down-spins enter into the same HOMO in conformity with formation of the stable covalent bond. Therefore spin degree of freedom (see Fig. S13) was freezed, namely out of concern in this situation. On the other hand, the HOMO-LUMO gap often becomes small for unstable  $M=O$  bond, indicating that the HOMO-LUMO mixing occurs when the gap becomes smaller than the on-site repulsion integral ( $U$ ) of metal ion to avoid strong electron repulsion effect as illustrated in Fig. S6. The up- and down-spins enter into the broken-symmetry (BS) localized orbitals, respectively, responsible for metal biradical state ( $\bullet M-O\bullet$ ) in chemical picture.

Nowadays, these BS chemical bonds are regarded as typical examples of SCES<sup>18</sup> where spin, charge and orbital degrees of freedom play important roles for emergence of their characteristic behaviors in both chemical reactions and material science (see Fig. S13). Past decades SCES has been accepted great

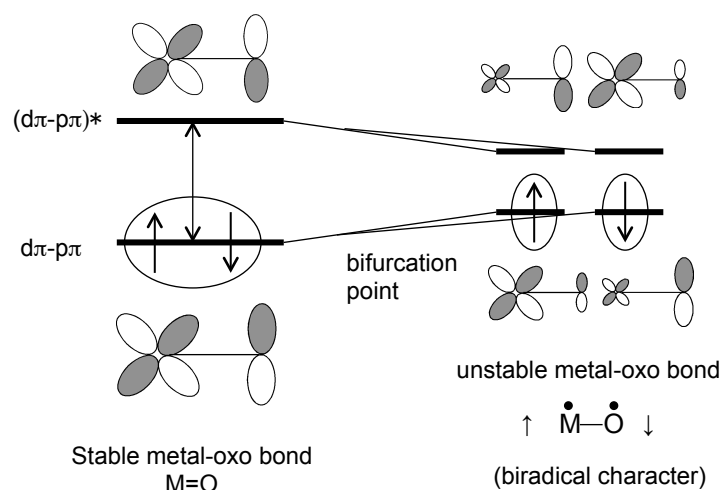


Fig. S6 The HOMO-LUMO mixing in the high-valent transition-metal oxo bond provides broken-symmetry (BS) orbitals responsible for local spins on the metal (M) and oxygen (O) sites, respectively<sup>44</sup>. The weight of the mixing is highly dependent on 3d, 4d and 5d metals. For example, it was large for the high-valent 3d metals such as Mn(X)=O (X=V, IV) and Fe(X)=O (X=V, IV), indicating large metal diradical character. On the other hand, the radical character was usually weak for 4d and 5d metals such as Ru(V)=O because of small HOMO-LUMO mixing<sup>44</sup>.

interest in physics, chemistry and chemical biology.<sup>10</sup> For example, the high-valent manganese-oxo bond Mn=O exhibited more or less MDR character ( $\bullet\text{Mn-O}\bullet$ ) in accord with its radical reactivity. Because of the MDR character of the high-valent manganese-oxo bonds, 1,4-metal diradical mechanism was indeed preferable to four-centered mechanism in the case of addition reaction of naked Mn(IV)=O to ethylene<sup>43</sup>. The MDR character ( $\bullet\text{M-O}\bullet$ )<sup>43</sup> is nowadays a theoretical foundation for the radical coupling (RC) mechanism for the O-O bond formation ( $\bullet\text{M-O}\bullet + \bullet\text{O-M}\bullet \rightarrow \bullet\text{M-O-O-M}\bullet$ ); M=Fe, Mn, Co, Ni, Cu).<sup>47</sup> On the other hand the MDR character was weak for the second- and third row transition metals oxo bonds such as Ru(V)=O, exhibiting the electrophilic reactivity.<sup>52</sup>

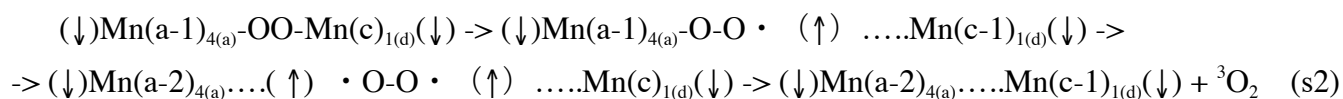
The metal-diradical character  $\bullet\text{M-O}\bullet$  is often reduced with participation of Lewis acid (L) even for 3d transition metals (M)<sup>65</sup>; M=O...L because of the increase of the HOMO-LUMO gap in Fig. S6. Moreover coordinated water molecules are contributable for reduction of the  $\bullet\text{M-O}\bullet$  character. For example, the Ca(II) ion in the CaMn<sub>4</sub>O<sub>5</sub> cluster is a typical example for such stabilization; Mn(IV)=O...Ca(II) as shown in the text. Therefore the Ca(II) ion plays an important role for the nonadiabatic (NA) one electron transfer (OET) mechanism (see Fig. S12). The left (L)-opened Mn<sub>a(4)</sub>=O species in OEC did not exhibit the metal diradical character because of hydrogen bonding stabilization<sup>15</sup> as shown in Table S1 (see later). On the other hand, the left (L)-opened excited Mn<sub>a(4)</sub> oxo\* species without such stabilization exhibited the metal diradical character (Mn-O $\bullet$ ). Therefore we must perform the natural orbital analysis for quantitative discussions on the radical coupling (RC) mechanisms for water oxidation on the basis of the QM/MM model including protein environments<sup>10</sup>.

### SII. 4 Spin correlation diagrams for radical coupling mechanism for O-O bond formation

Orbital correlation diagrams are often used for elucidation of orbital symmetry allowed and forbidden reactions on the theoretical grounds. Extended Huckel MO (EHMO) models neglecting spin degree of freedom work well for depicting the orbital correlation diagram that is characterized by the spatial symmetry ( $P_n$ ). On the other hand, both orbital and spin degrees of freedom play important roles for broken-symmetry (BS) approach for chemical reactions. For example, spin correlation diagrams are useful for elucidation of exchange allowed and forbidden radical reactions.<sup>47</sup> The HOMO-LUMO mixing occurs in the case of 3d-3d molecular orbitals of the  $\text{CaMn}_4\text{O}_5$  cluster, providing local spins on the Mn ions responsible for eight spin alignments mentioned above. Spin Hamiltonian models<sup>32,69</sup> are often employed for elucidation of the spin correlation diagram that is characterized by the magnetic group ( $S \times T$ ) where S and T means spin rotation and time-reversal symmetries, respectively.<sup>46</sup>

The up- and down-spins are often expressed by arrow notations ( $\uparrow$ ) and ( $\downarrow$ ) in chemistry, respectively. For example, the spin correlation diagram was depicted for water oxidation in the  $\text{CaMn}_4\text{O}_5$  cluster of OEC of PSII as illustrated in Fig. S7. The corresponding broken-symmetry (BS) solutions for these spin structures can be constructed on the basis of the magnetic double group theory ( $S \times T \times P_n$ ).<sup>46</sup>

The formation of high-valent  $\text{Mn(IV)}_{a(4)}\text{-oxo}$  ( $\text{Mn(IV)}_{a(4)}=\text{O}$ ) bond becomes feasible even in the  $S_3$  state via the equilibrium reaction;  $\text{Mn(IV)(OH)}_2 \leftrightarrow \text{Mn(IV)=O(H}_2\text{O)}$ .<sup>41</sup> Therefore the  $\text{Mn}_{a(4)}\text{-O-O}_{(5)}$  bond formation is conceivable even in the  $S_3$  state as an initial step for water oxidation followed by the internal conversion from the left- to right-opened structure (see Fig. S19). However, the radical coupling (RC) process proposed in 2010<sup>47</sup> was very simple (no internal conversion) as follows. The local up ( $\uparrow$ )-spin of the terminal oxygen atom is exchange-coupled with the local down ( $\downarrow$ ) spin of the  $\text{O}_{(5)}$  atom in the intermediary stage (**3**) in Fig. s7, showing the formation of the local singlet diradical (LSD) configuration that easily undergoes the O-O coupling to afford the metal peroxide;  $\text{Mn-OO-Mn}$ .<sup>47</sup> On the other hand, the local ferromagnetic configuration ( $\downarrow\downarrow$ ) between the  $\text{Mn}(a-1)_{4(a)}$  and  $\text{Mn}(c)_{1(d)}$  sites plays an important role for generation of triplet molecular oxygen ( $\uparrow\uparrow$ ) as follows.



In this simple O-O coupling model, the  $\text{Mn}_{4(a)}$  site is totally two-electron reduced, showing the necessity of a typical high-valent valence configuration  $\text{Mn(V)}$ . This may in turn indicate that strong oxidation reagents such as  $\text{Ce(IV)}$  becomes crucial for water oxidation in many artificial systems.<sup>50-54</sup> On the other hand, formation of the high-valent  $\text{Mn(V)}_{4(a)}$  site is not necessary if the  $\text{Mn}_{a(4)}\text{-O-O}_{(5)}\text{-Mn}_{1(d)}$  bond formation occurs in the  $S_3$  state followed by the internal conversion into the  $\text{Mn}_{a(4)}\text{-O}_{(5)}\text{-O-Mn}_{1(d)}$  as mentioned above. One electron oxidation of the  $\text{CaMn}_4\text{O}_5$  cluster proceeds through  $\text{tyr-O} \cdot$  radical in OEC of PSII, indicating almost constant oxidation potential. Thus the O-O bond formation in the  $S_3$  state remains as a possible scenario for water oxidation. However, it is noteworthy that the valence configuration of the (4444) or (4443) is converted into the (3443) or (3343) after the O-O bond formation

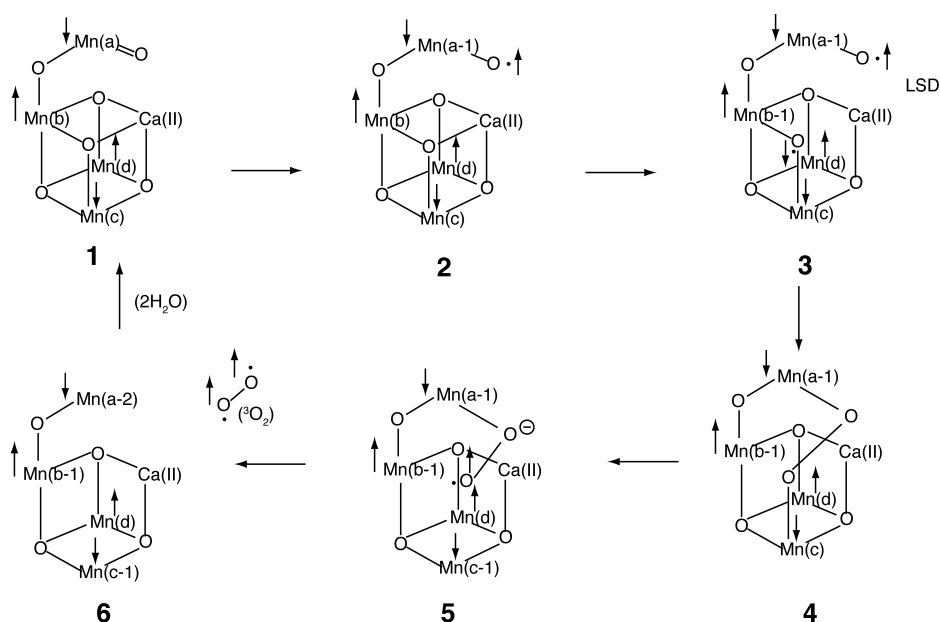


Fig. S7 Spin correlation diagrams for the O-O bond formation and release of triplet molecular oxygen for water oxidation in OEC of PSII. LSD denotes the local singlet diradical (LSD) configuration.

in contradiction to the XES results.<sup>5-7</sup> The spin correlation diagram in Fig. S7 is equally applicable for the OO bond formation in the  $S_4$  state.<sup>47</sup>

### SII. 5 Nonadiabatic one electron transfer mechanism for water oxidation

Water insertion is crucial for water oxidation in the  $S_3$  to  $S_4$  transition even though no water insertion in the  $S_2$  to  $S_3$  transition in OEC of PSII. The non-innocent organic radicals such as Tyr-O· radical may play an important role for nonadiabatic (NA) one electron transfer (OET) reaction for water oxidation. Figures S8 and S9 illustrate possible one electron transfer (OET) processes for water oxidation in OEC of PSII where Tyr-O· radical acts effectively as one electron acceptor for the one electron donor;  $\text{CaMn}_4\text{O}_5$  cluster. This means that non-innocent radical species are effective for construction of artificial photosynthetic (AP) systems without sacrificial reagents.<sup>33, 62, 63</sup>

Figure S8 illustrates the O-O bond formation in the  $S_3$  to  $S_4$  transition where the insertion of W3 is assumed to occur at the  $\text{Mn}_{a(4)}$  site in the initial stage of the water oxidation. The isomerization of the initially formed  $\text{Mn}_{a(4)}(\text{OH})_2$  species into  $(\text{H}_2\text{O})\text{Mn}_{a(4)}=\text{O}$  species is considered to generate the high-valent  $\text{Mn}_{a(4)}=\text{O}$  bond that can undergo the  $\text{Mn}_{a(4)}-\text{O}-\text{O}_{(5)}-\text{Mn}_{d(1)}$  bond formation (see “in the intermediate correlation regime” in Table S1). The internal conversion<sup>15</sup> from peroxo (L) species  $\text{Mn}_{a(4)}-\text{O}-\text{O}_{(5)}-\text{Mn}_{d(1)}$  to peroxo (R) species  $\text{Mn}_{a(4)}-\text{O}_{(5)}-\text{O}-\text{Mn}_{d(1)}$  is not depicted in Fig. S8.  $\text{S}_\text{N}2$  substitution reaction of superoxide anion  $\text{O}_{(5)}-\text{O}\cdot$  with hydroxide anion at W2 site was assumed to reproduce the  $S_0$  structure. Two water molecules are inserted at the final stage in accord with the Kok cycle in Fig. S2.

Figure S9 illustrates the O-O bond formation in the  $S_3$  to  $S_4$  transition where the insertion of W3 is

assumed to occur at the  $Mn_{a(4)}$  site in the initial stage of the water oxidation. Instead of the O-O bond formation, the proton-transfer from a newly formed OH<sup>-</sup> to the  $O_{(5)}$  site (see “in the weak correlation regime in Table S1”) was assumed to generate the right (R)-opened OH<sup>-</sup> inserted structure that is converted into the  $Mn_{d(1)}$ -oxo species.<sup>16</sup> The  $Mn_{d(1)}=O$  bond can undergo the O-O bond formation, directly providing the peroxy (R) species  $Mn_{a(4)}-O_{(5)}-O-Mn_{d(1)}$ . SN<sub>2</sub> substitution reaction of superoxide anion  $O_{(5)}-O \cdot$  with hydroxide anion at W2 site was assumed to reproduce the  $S_0$  structure. Two water molecules are inserted at the final stage in accord with the Kok cycle in Fig. S2.

Several similar pathways are conceivable since several water inlet pathways are feasible for initial insertion of water molecule at the  $Mn_{a(4)}$  site as illustrated in Fig. S21 (see later). The key concept is the OO bond formation like in the case of Fig. S8 and S9 instead of the O-OH bond formation examined in Figs. S3-S5. However, reaction pathways might be dependent on hybrid DFT (HDFT) functionals employed for locations of possible intermediates and transition structures since relative stabilities of key structures are highly dependent on electron correlations as summarized in Table S1 (see later). Figures S10 and S11 illustrate the fully optimized geometries of the Mn-O-O-Mn intermediates formed in the left (L) and right (R) handed pathways in the  $S_4$  state. The optimized OO distances are about 1.3 Å. Figure S12 illustrates the orbital interaction diagrams for formal acid-base (O-OH), radical coupling (O-O) (RC) and non-adiabatic (NA) one-electron transfer (CT) mechanisms for water oxidation. It is noteworthy that the diradical characters are variable for all these mechanisms, depending on environmental effects.<sup>65</sup>

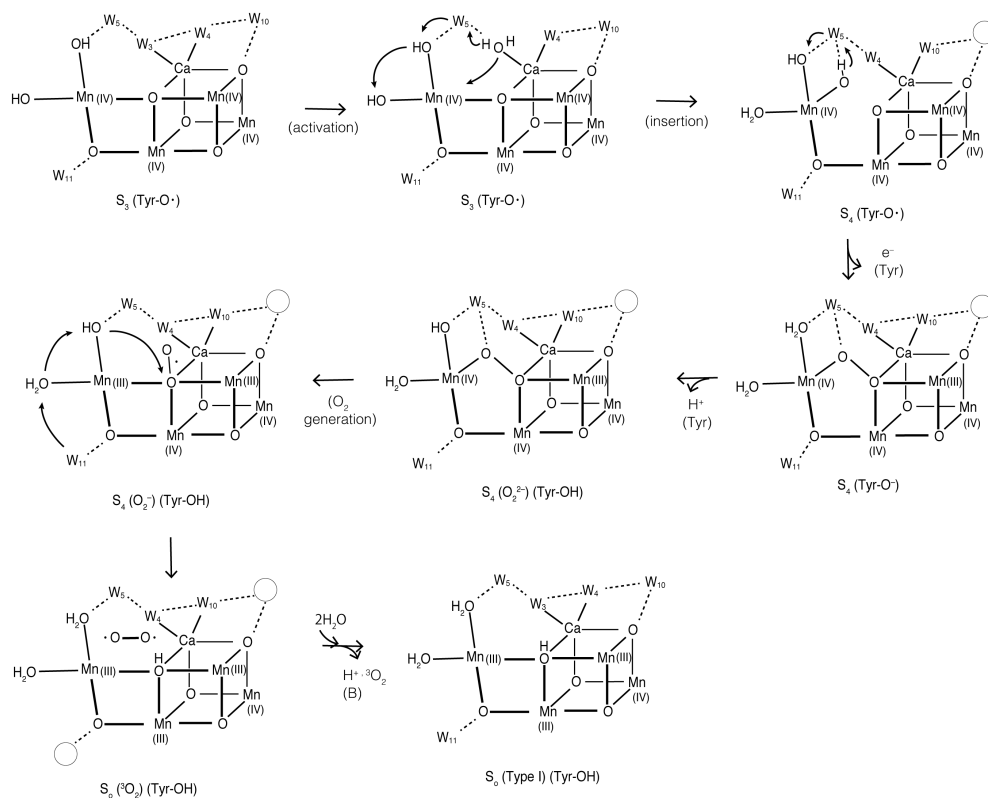


Fig. S8 Possible left (L)-opened O-O coupling pathway for water oxidation in OEC of PSII<sup>44</sup>.

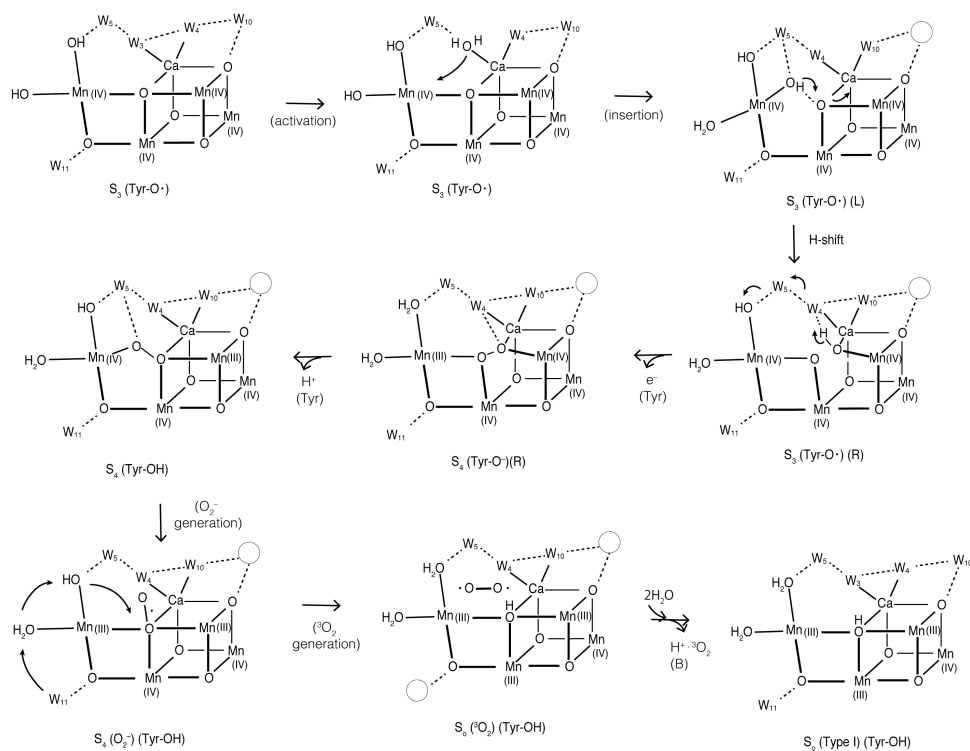


Fig. S9 Possible right (R)-opened O-O coupling pathway for water oxidation in OEC of PSII<sup>44</sup>.

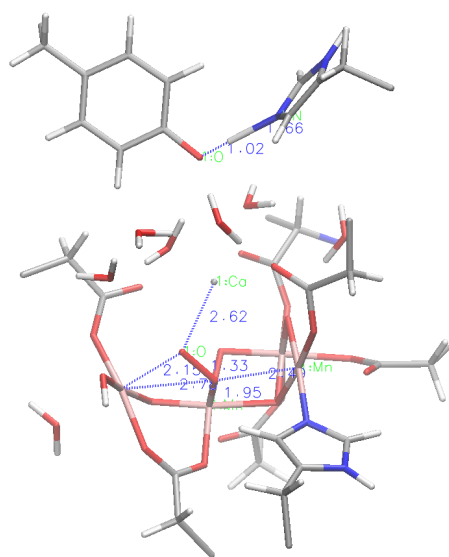


Figure S10 Full geometry optimized structure of  $S_4(\text{O}_2^{2-})(\text{Tyr-OH})$  in Fig. S8. Its valence state is described as  $\text{Ca(II)Mn(IV)}_{a(4)}\text{Mn(IV)}_{b(3)}\text{Mn(IV)}_{c(2)}\text{Mn(III)}_{d(1)}$  that is referred to as (4443).

The O-O distance is 1.33 Å, that is consistent with that of molecular oxygen dianion.

The  $\text{Mn}_{a(4)}\text{-O}_{(5b)}$  and  $\text{Ca-O}_{(5b)}$  distances are 2.15 and 2.62 (Å), respectively. The  $\text{Mn}_{a(4)}\text{-O}_{(5a)}$  distance is 2.7 (Å), indicating the right (R)-opened structure.

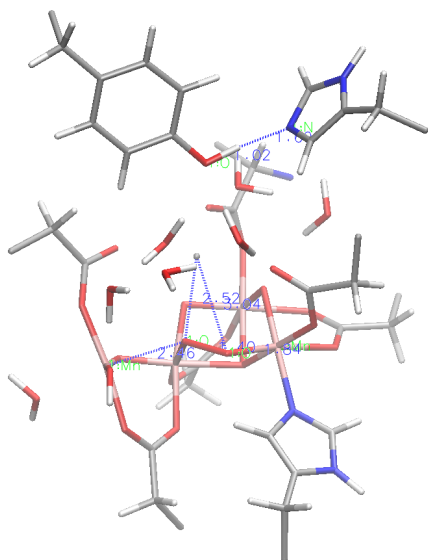
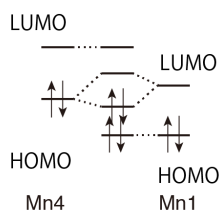
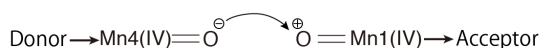
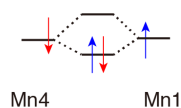
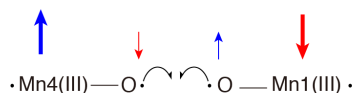


Figure S11 Full geometry optimized structure of  $S_4(O_2^{2-})(Tyr-OH)$  in Fig. S9. Its valence state is described as  $Ca(II)Mn(III)_{a(4)}Mn(IV)_{b(3)}Mn(IV)_{c(2)}Mn(IV)_{d(1)}$  that is referred to as (3444). The  $Ca-O_{(5b)}$  distance is 2.52 Å. The  $Mn_{a(4)}-O_{(5a)}$  distance is 2.46 (Å), indicating the right (R)-opened structure.

### Acid-base



### RC



### NA-CT

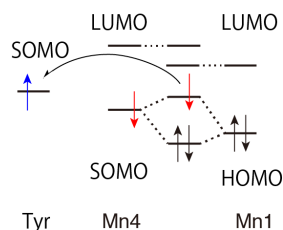
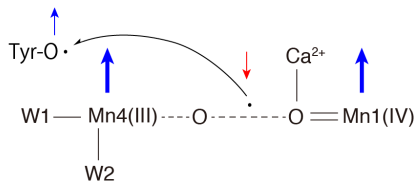


Figure S12 Orbital interaction diagrams for the O-O bond formation via three different mechanisms: (i) acid-base, (ii) simple radical coupling (RC) and nonadiabatic (NA) charge-transfer (CT) that is equivalent to one electron transfer (OET). These mechanisms are highly dependent on environmental effects and geometrical structures of the  $CaMn_4O_5$  cluster. Therefore the XFEL structures of the  $S_3$  and  $S_4$  states are crucial for elucidation of the mechanism of water oxidation in OEC of PSII.

### SIII Relative stabilities of possible intermediates in the $S_3$ state

#### SIII. 1 Strongly correlated electron systems and artificial photosynthesis

Our fundamental physical view of the oxygen evolving complex (OEC) of photosystem II (PSII) is that the  $\text{CaMn}_4\text{O}_5$  cluster in OEC of PSII is a typical strongly correlated electron system (SCES)<sup>33</sup>, where electron-electron repulsion effect plays an important role for determination of orbital, electronic and spin structures as illustrated in Fig. S13 ( K. Yamaguchi et al, Mol. Phys. 115, 636 (2017)). For example, eight different spin structures for the  $\text{Mn}_4$  cluster are conceivable for spin degree of freedom in the  $\text{CaMn}_4\text{O}_5$  cluster.<sup>32</sup> On the other hand six different mixed -valence (MV) configurations are feasible for charge degree of freedom in the  $\text{Ca(II)Mn(III)}_2\text{Mn(IV)}_2$  cluster in the  $S_1$  state of OEC of PSII. Therefore total  $8 \times 6 = 48$  broken-symmetry (BS) configurations are available for the  $S_1$  state, indicating that the electronic and spin structures of OEC of PSII are expressed by the linear combination of 48 BS solutions where the expansion coefficients are determined by  $48 \times 48$  BS configuration interaction (CI) technique.<sup>34</sup> The main configuration for the ground state of the  $S_1$  state was found to be  $\text{Ca(II)Mn(III)}_{a(4)}\text{Mn(IV)}_{b(3)}\text{Mn(IV)}_{c(2)}\text{Mn(III)}_{d(1)}$  that is abbreviated as the (3443) configuration.

The  $\text{Mn(III)}_{a(4)}$  ion is a typical Jahn-Teller (JT) ion where the orbital degree of freedom plays an important role for subtle deformations of geometrical structures of the  $\text{CaMn}_4\text{O}_5$  cluster. For example, the JT elongation axis may rotate from the vertical (v) (to the  $\text{Mn}_{a(4)}\text{-O}_{(5)}\text{-Mn}_{d(1)}$  axis)) orientation to the horizontal (h) (to the same axis) orientation, depending on the strength of ligand fields for the  $\text{Mn(III)}_{a(4)}$  ion. The magnitude of nuclear motion is sensitive to the types of ligands as illustrated in Fig. S13. The packing structures of the crystals of PSII may be also responsible for subtle changes of the JT elongation axis. It is noteworthy that the packing structures of PSII were different between the samples by Berkeley and Okayama groups.

As mentioned above, our view of OEC of PSII is a SCES confined with protein fields as illustrated in Fig. S14.<sup>18</sup> The SCES in OEC selected by Nature was the Ca-doped Mn oxide cluster; the  $\text{CaMn}_4\text{O}_5$  cluster. However, the nature of the chemical bonds of the  $\text{CaMn}_4\text{O}_5$  cluster in OEC of PSII is labile, indicating the necessity of re-construction of the cluster after the damage. Therefore the protein fields should be replaced with robust confinement materials in artificial photosynthesis (AP) since repairing function of OEC is hardly imitated with AP systems. Previously,<sup>18</sup> we proposed several confinements materials such as metal organic framework (MOF), polyoxo metallate (POM), nano tube (NT). The  $\text{CaMn}_4\text{O}_5$  cluster as a SCES may be also replaced with other 3d abundant metal clusters (M=Ti, V, Cr, Fe, Co, Ni, Cu) since adjustments of redox potentials are crucial for water oxidation reaction without sacrificial reagents. Thus theoretical studies of OEC of PSII have provided a guiding principle for design of AP systems as illustrated in Fig. S14; namely

*“ different 3d transition metal clusters for different artificial robust ligands in efficient AP”.*

Basic concept: Four important degrees of freedom in strongly correlated electron systems (SCES)

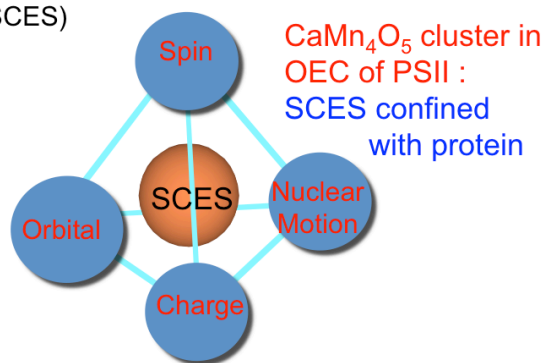


Fig. S13 Four degrees of freedom for strongly correlated electron systems (SCES).

### Our picture of OEC of PSII Confinements of SCES by several reaction fields

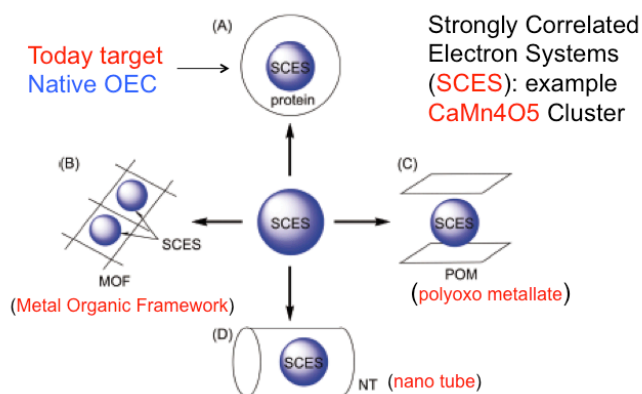


Fig. S14 Design of artificial photosystems (AP) consisted of SCES and confinement materials.

### SI.2 The Mn-Mn and Ca-Mn distances for possible intermediates in the S<sub>3</sub> state

Hybrid density functional theory (HDFT) methods are usually applicable for geometry optimizations of SCES such as 3d transition metal inorganic complexes since geometries of SCES are mainly determined with population of densities. On the other hands, metalloenzymes are regarded as SCES confined with proteins, often indicating strong coupling between SCES and proteins. Nowadays, the QM/MM method is a standard and well-accepted approach for theoretical modeling of such complex systems. As shown in section SI.1, we performed large-scale QM (HDFT)/MM calculations of possible intermediates with and without insertion of water molecule in the S<sub>3</sub> state of OEC of PSII. The optimized Mn-Mn and Ca-Mn distances by large-scale QM/MM were thoroughly examined in the text. We have schematically depicted characteristic features elucidated by QM/MM in Figs. S15 and S16 for comparison with the experimental results by Berkeley and Okayama groups (see Figs. S17 and S18) (see the discussion section of the Faraday conference for AP in the text).

Figure S15 illustrated the optimized  $\text{Mn}_{a(4)}\text{-Mn}_{b(3)}$  and  $\text{Mn}_{a(4)}\text{-Mn}_{d(1)}$  distances (bold faces were employed for pictorial expressions of them) of the left-opened (L) geometries in the  $S_2$  and  $S_3$  states of OEC of PSII by large-scale QM/MM.<sup>10</sup> The key points are that (i) the  $\text{Mn}_{a(4)}\text{-Mn}_{b(3)}$  distances are about 3.1 Å before the insertion of hydroxide anion ( $\text{OH}^-$ ) in both  $S_2$  and  $S_3$  states, (ii) the  $\text{Mn}_{a(4)}\text{-Mn}_{b(3)}$  distances are elongated by about 0.1 Å after the insertion of hydroxide anion ( $\text{OH}^-$ ), (iii) the  $\text{Mn}_{a(4)}\text{-Mn}_{d(1)}$  distances are about 5.0 Å before the insertion of hydroxide anion ( $\text{OH}^-$ ), and (iv) the  $\text{Mn}_{a(4)}\text{-Mn}_{d(1)}$  distances are elongated by about 0.3 Å after the insertion of hydroxide anion ( $\text{OH}^-$ ).

Figure S16 illustrated the optimized  $\text{Mn}_{b(3)}\text{-Mn}_{d(1)}$  and  $\text{Mn}_{a(4)}\text{-Mn}_{d(1)}$  distances (bold faces were employed for pictorial expressions of them) of the right-opened (R) geometries in the  $S_2$  and  $S_3$  states of OEC of PSII. The key points are that (i) the  $\text{Mn}_{b(3)}\text{-Mn}_{d(1)}$  distances are about 3.35 Å before the insertion of hydroxide anion ( $\text{OH}^-$ ) in both  $S_2$  and  $S_3$  states, (ii) the  $\text{Mn}_{b(3)}\text{-Mn}_{d(1)}$  distances are elongated by about 0.2 Å after the insertion of hydroxide anion ( $\text{OH}^-$ ), (iii) the  $\text{Mn}_{a(4)}\text{-Mn}_{d(1)}$  distances are about 4.95 Å before the insertion of hydroxide anion ( $\text{OH}^-$ ), (iv) the  $\text{Mn}_{a(4)}\text{-Mn}_{d(1)}$  distances are elongated by about 0.35 Å after the insertion of hydroxide anion ( $\text{OH}^-$ ), (v) the  $\text{Ca(II)}\text{-Mn}_{a(4)}$  distances are about 3.88 Å before the insertion of hydroxide anion ( $\text{OH}^-$ ), and (vi) the  $\text{Ca(II)}\text{-Mn}_{a(4)}$  distances are elongated by about 0.15 Å after the insertion of hydroxide anion ( $\text{OH}^-$ ).

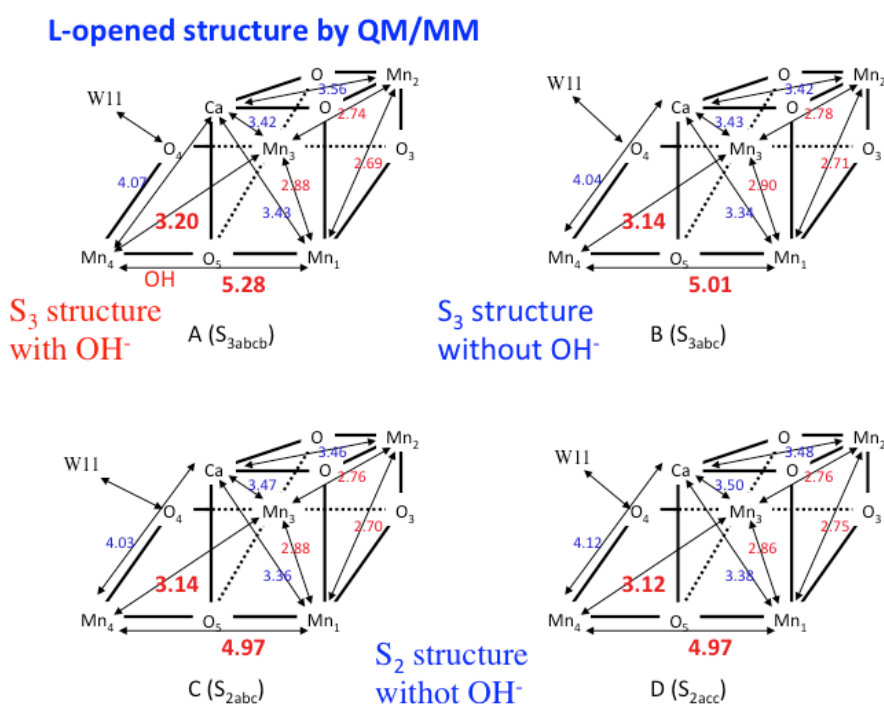


Figure S15 The optimized Mn-Mn and Ca-Mn distances for left-opened (L) structure by large-scale QM/MM calculations.<sup>10</sup> The average  $\text{Mn}_{4(a)}\text{-Mn}_{3(b)}$ ,  $\text{Mn}_{3(b)}\text{-Mn}_{2(c)}$  and  $\text{Mn}_{2(c)}\text{-Mn}_{1(d)}$  distances are 2.88 Å for A, B, and D, and 2.87 Å for C, indicating no difference between the  $S_2$  and  $S_3$  structures

### R-opened structure by QM/MM

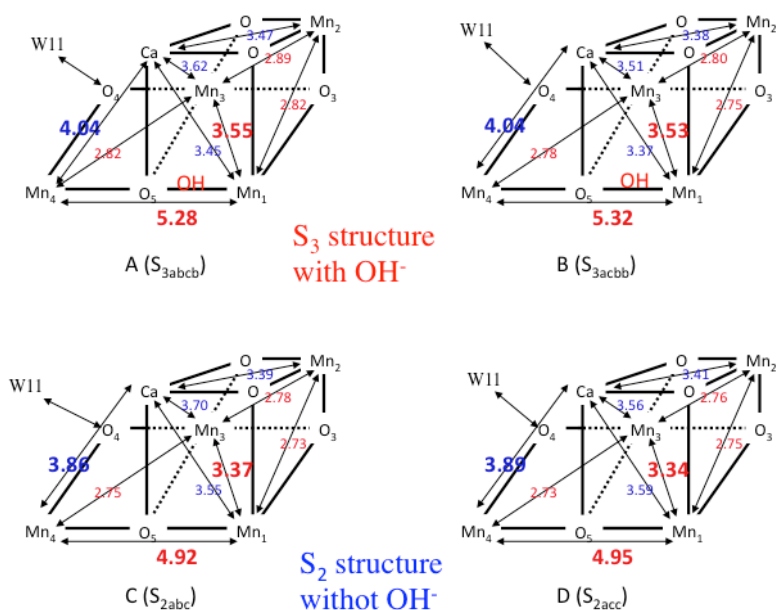


Figure S16 The optimized Mn-Mn and Ca-Mn distances for right-opened (R) structure by large-scale QM/MM calculations.<sup>10</sup> The average  $Mn_{4(a)}-Mn_{3(b)}$ ,  $Mn_{3(b)}-Mn_{2(c)}$  and  $Mn_{2(c)}-Mn_{1(d)}$  distances are 2.84, 2.78, 2.76 and 2.75 (Å) for A, B, C and D, respectively, indicating a slight elongation with the  $OH^-$  insertion at the  $S_2 \rightarrow S_3$  transition.

Figure S17 illustrated the  $Mn_{a(4)}-Mn_{b(3)}$ ,  $Mn_{b(3)}-Mn_{d(1)}$  and  $Mn_{a(4)}-Mn_{d(1)}$  distances of the intermediates in the  $S_1$  and  $S_3$  states of OEC of PSII revealed by serial femtosecond X-ray-diffraction (SFX) technique (I. Young et al., Nature 540, 453-457 (2016)). The key points are that (i) the  $Mn_{a(4)}-Mn_{d(1)}$  distance is about 4.9 Å in both  $S_1$  and  $S_3$  states, (ii) the  $Mn_{a(4)}-Mn_{d(1)}$  distance is not elongated in the  $S_1$  to  $S_3$  (the sample after two flash irradiation) transition, (iii) the  $Mn_{b(3)}-Mn_{d(1)}$  distance is about 3.2 Å in both  $S_1$  and  $S_3$  states, (iv) the  $Mn_{b(3)}-Mn_{d(1)}$  distance is not elongated in the  $S_1$  to  $S_3$  transition, (v) the  $Mn_{a(4)}-Mn_{b(3)}$  distance is about 2.8~2.9 Å in both  $S_1$  and  $S_3$  states, and (vi) the  $Mn_{a(4)}-Mn_{d(1)}$  distance is not elongated in the  $S_1$  to  $S_3$  transition. From these experimental results, Berkeley group has concluded no insertion of hydroxide anion in the  $S_1$  to  $S_3$  transition.

The  $Mn_{a(4)}-Mn_{b(3)}$  distance (about 2.8~2.9 Å) in the  $S_3$  state by the SFX experiment by Berkeley group is consistent with the corresponding value of the right-opened (R)- $S_3$  structure by large-scale QM/MM in Fig. S16. However, the SFX structure did not indicate the elongation (about 0.2 Å) of the  $Mn_{b(3)}-Mn_{d(1)}$  distance and elongation (0.35 Å) of the  $Mn_{a(4)}-Mn_{d(1)}$  distance after the  $OH^-$  insertion expected by QM/MM. This may in turn support the conclusion of Berkeley group, namely no insertion

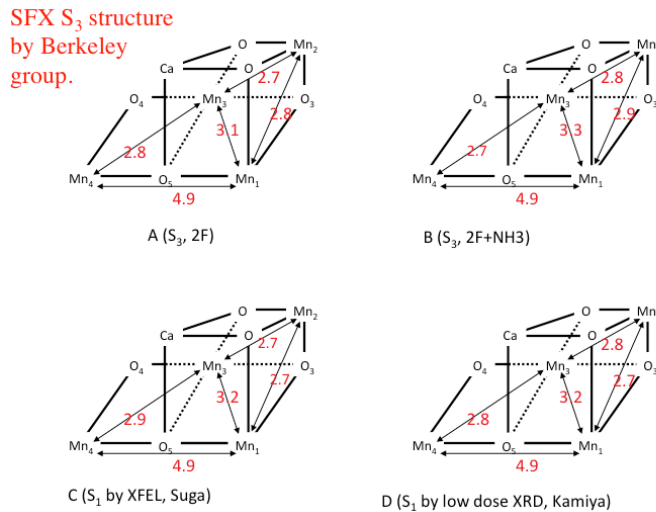


Figure S17 The Mn-Mn distances of the  $S_3$  structure with the SFX experiments by the Berkeley group (I. Young et al., Nature 540, 453-457 (2016)). The sum of the  $Mn_{a(4)}-Mn_{b(3)}$ ,  $Mn_{b(3)}-Mn_{d(1)}$  and  $Mn_{a(4)}-Mn_{d(1)}$  distances are 8.3 Å for A, B, C and 8.4 Å for D, respectively, indicating no difference between  $S_2$  and  $S_3$ .

of the  $OH^-$  anion in the  $S_1$  to  $S_3$  transition in OEC of PSII. Berkeley group further performed the SFX experiments on the  $NH_3$  addition sample as shown in Fig. S17. The  $Mn_{a(4)}-Mn_{b(3)}$ ,  $Mn_{b(3)}-Mn_{d(1)}$  and  $Mn_{a(4)}-Mn_{d(1)}$  distances of the 2F+ $NH_3$  sample are not so different from the corresponding values of the sample without  $NH_3$ .

Figure S18 illustrated the  $Mn_{a(4)}-Mn_{b(3)}$ ,  $Mn_{b(3)}-Mn_{d(1)}$  and  $Mn_{a(4)}-Mn_{d(1)}$  distances of the intermediates in the  $S_1$  and  $S_3$  states of OEC of PSII revealed by X-ray free electron laser (XFEL) technique (Suga et al., Nature 543, 131-135 (2017)). The key points are that (i) the  $Mn_{a(4)}-Mn_{d(1)}$  distance is about 5.0 Å in both  $S_1$  and  $S_3$  states, (ii) the  $Mn_{a(4)}-Mn_{d(1)}$  distance is not elongated in the  $S_1$  to  $S_3$  (the sample after two flash irradiation) transition, (iii) the  $Mn_{b(3)}-Mn_{d(1)}$  distances are about 3.20 and 3.27 (Å) in the  $S_1$  and  $S_3$  states, respectively, (iv) the  $Mn_{b(3)}-Mn_{d(1)}$  distance is slightly elongated (0.07 Å) in the  $S_1$  to  $S_3$  transition, (v) the  $Mn_{a(4)}-Mn_{b(3)}$  distances are 2.98 and 2.94 (Å), respectively, in the  $S_1$  and  $S_3$  states of the A monomer of OEC of PSII, (vi) the  $Mn_{a(4)}-Mn_{d(1)}$  distance of the A monomer is almost constant in the  $S_1$  to  $S_3$  transition, (vii) the  $Mn_{a(4)}-Mn_{b(3)}$  distances are 2.91 and 2.83 (Å), respectively, in the  $S_1$  and  $S_3$  states of the B(a) monomer of OEC of PSII, and (vi) the  $Mn_{a(4)}-Mn_{b(3)}$  distance of the B(a) monomer is a little shortened (0.08 Å) in the  $S_1$  to  $S_3$  transition.

The above characteristic behaviors of OEC of PSII by XFEL are different from the conclusions by large-scale QM/MM in Fig. S16. Interestingly, the XFEL results by Okayama group indicated different behaviors of the A and B(a) monomers in the dimer structure of the OEC of PSII. The  $Mn_{a(4)}-Mn_{d(1)}$  distance of the  $S_3$  structure was not elongated as shown in Fig. S16 in contradiction to the elongation by 0.3 Å revealed by large-scale QM/MM. This may suggest that other  $S_3$  structures instead of the right-(R) opened  $S_3$  structure with the inserted  $OH^-$  in Fig. S16 might be formed in the  $S_1$  to  $S_3$  transition.

### S<sub>3</sub> structure by the XFEL experiments (Suga et al, Nature 2017)

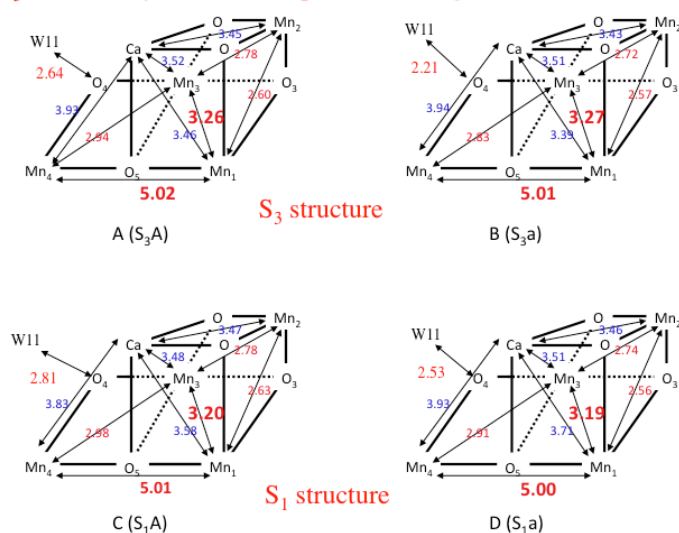


Figure S18 The Mn-Mn and Ca-Mn distances of the S<sub>3</sub> structure with the XFEL experiments by the Okayama group (Suga et al, Nature 543, 131 (2017)). The average Mn<sub>4(a)</sub>-Mn<sub>3(b)</sub>, Mn<sub>3(b)</sub>-Mn<sub>2(c)</sub> and Mn<sub>2(c)</sub>-Mn<sub>1(d)</sub> distances are 2.77, 2.71, 2.80 and 2.77 (Å) for A, B, C and D, respectively, indicating a slight shortening with the water insertion at the S<sub>2</sub> → S<sub>3</sub> transition.

Further theoretical investigation of possible several intermediates in the S<sub>3</sub> state is now crucial for understanding of the SFX results at room temperature. This is our reply for possible roles of the O<sub>(5)</sub> site in the S<sub>3</sub> state in the questions 200 and 203 in the Faraday Discussion.

### SII. 3 Full geometry optimizations of possible intermediates in the S<sub>3</sub> state of OEC of PSII

The SFX results by Suga et al (Nature 543, 131 (2017)) have indicated the necessity of further theoretical investigation of possible intermediates in the S<sub>3</sub> state. Isobe et al.<sup>15</sup> already performed full geometry optimizations of the intermediates in the S<sub>3</sub> state of OEC of PSII as shown in Fig. S19. The following characteristics are shown:

- (i) The right-opened structure with the inserted OH<sup>-</sup> at the Mn<sub>d(1)</sub> site exhibited the hydrogen-bonding characteristic; Mn<sub>a(4)</sub>-O<sub>(5)</sub>...H-O<sub>(6)</sub>-Mn<sub>d(1)</sub>, showing that the O<sub>(5)</sub>-O<sub>(6)</sub> distance becomes longer than 2.5 Å in contradiction to the observed value (about 1.5 Å) by the XFEL experiment (Reply to the questions 232-234). The Mn<sub>b(3)</sub>-Mn<sub>d(1)</sub> distance was 3.54 Å, indicating an elongation of about 0.2 Å.
- (ii) The left-opened structure with the inserted OH<sup>-</sup> at the Mn<sub>a(4)</sub> site was also examined, exhibiting hydrogen-bonding characteristic; Mn<sub>a(4)</sub>-O<sub>(6)</sub>-H...O<sub>(5)</sub>-Mn<sub>d(1)</sub> where the O<sub>(5)</sub>-O<sub>(6)</sub> distance becomes longer than 2.5 Å.
- (iii) The right-opened structure with the inserted oxo/oxyl at the Mn<sub>d(1)</sub> site exhibited no hydrogen-bonding characteristic; Mn<sub>a(4)</sub>-O<sub>(5)</sub>...O<sub>(6)</sub>=Mn<sub>d(1)</sub>, showing that the O<sub>(5)</sub>-O<sub>(6)</sub> distance becomes 1.96 Å that

is a little longer than the observed value (about 1.5 Å) by the XFEL experiment. The  $Mn_{b(3)}-Mn_{d(1)}$  distance was 3.35 Å, indicating no elongation in the  $S_1$  to  $S_3$  transition.

(iv) The left-opened structure with the inserted oxo/oxyl at the  $Mn_{a(4)}$  site exhibited a reverse bonding pattern,  $Mn_{a(4)}=O_{(6)}\cdots O_{(5)}-Mn_{d(1)}$ , showing that the  $O_{(5)}-O_{(6)}$  distance also becomes 1.9~2.0 Å.

(v) The right-opened structure with the inserted peroxo species exhibited a bonding characteristic;  $Mn_{a(4)}-O_{(5)}-O_{(6)}-Mn_{d(1)}$ , showing that the  $O_{(5)}-O_{(6)}$  distance becomes 1.41 Å that is compatible with the observed value (about 1.5 Å) by XFEL. The  $Mn_{b(3)}-Mn_{d(1)}$  distance was 3.32 Å, indicating no elongation.

(vi) The left-opened structure with the inserted peroxo species exhibited a bonding characteristic;  $Mn_{a(4)}-O_{(5)}-O_{(6)}-Mn_{d(1)}$ , showing that the  $O_{(5)}-O_{(6)}$  distance becomes 1.4~1.5 Å.

(vii) The quasi-central structure with the inserted superoxo species exhibited a bonding characteristic;  $Mn_{a(4)}-[O_{(5)}-O_{(6)}]-Mn_{d(1)}$ , showing that the  $O_{(5)}-O_{(6)}$  distance becomes 1.32 Å that is also compatible with the observed value (about 1.5 Å) by XFEL. The  $Mn_{b(3)}-Mn_{d(1)}$  distance was 3.44 Å, indicating a little elongation of 0.1 Å.

Suga et al (Nature 543, 131 (2017)) have pointed a formation of peroxo and/or superoxo bond in the  $S_3$  structure by their XFEL experiment. The observed XFEL structure was certainly consistent with the optimized geometrical parameters in the above (v) and (vii) (Reply to the questions 232-234). The possibility of O-O bond formation in the  $S_3$  state has been a classic problem provided by Renger<sup>61</sup> (Journal of Photochemistry and Photobiology B: Biology 104, 35 (2011) since electron-transfer (ET) dynamics experiments by his group have indicated the maximum activation barrier in the  $S_3$  state. Therefore systematic theoretical investigation involving the ET dynamics is now inevitable to elucidate possible mechanisms of the O-O bond formation in the  $S_3$  state ( or  $S_3 + tyr-O \cdot$  state after the third flash, namely formally the  $S_4$  state in Fig. S2). This is in accord with the necessity of dynamics emphasized in the questions 201 and 202 by Prof. Harriman. In the discussion section of Faraday conference, I (K. Y.) did not provide answer(s) for the question “how about the mechanism of the O-O bond formation ? (the questions 203 and 233) ” presented by Prof. Sun. My opinion is that the problem was not solved on the theoretical grounds yet. The XFEL results by Young et al. (Nature 540, 453-457 (2016)) and Suga et al. (Nature 543, 131-135 (2017)) opened a new door to enter an unexplored area in the O-O bond formation for water oxidation in OEC of PSII. In this paper we have explained three possible mechanisms for water oxidation on the basis of the XRD and XFEL structures as shown in Fig. S12. Further theoretical investigations are necessary for elucidation of possible intermediates in the  $S_3$  and  $S_4$  states.

Very recently Kamiya et al. (J. Am. Chem. Soc. 139, 1718 (2017) ) have elucidated two subtle different structures for the A- and B-monomers, respectively, in the  $S_1$  state of OEC of PSII by very low doze high-resolution XRD method, demonstrating important roles of hydrogen bonding interactions at the  $O_{(4)}$  and  $O_{(3)}$  sites of the  $CaMn_4O_5$  cluster for active controls by protein fields. Suga et al also demonstrated the different hydrogen bonding interactions at the  $O_{(4)}$  site between A- and B-monomers in

the  $S_3$  state. The experimental evidence clearly indicates the necessity of further large-scale QM/MM calculations for elucidation of possible roles of protein environments for water oxidation in OEC of PSII.

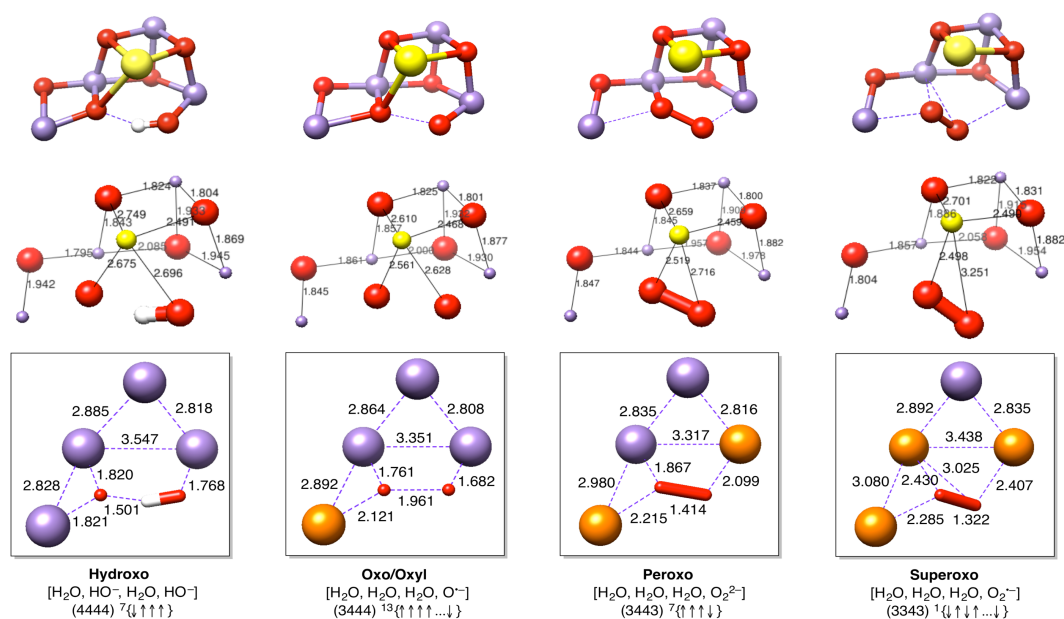


Figure S19 The optimized geometrical structures by large-scale QM methods.<sup>15</sup>

#### SII. 4 Variations of relative stabilities of possible intermediates in the $S_3$ state of OEC of PSII

As shown in the preceding section, hybrid density functional theory (HDFT) methods provide reasonable geometrical parameters of several possible intermediates in the  $S_3$  state of OEC of PSII. However, it should be very careful to discuss relative stabilities among the possible intermediates based on the HDFT methods since HDFT often provide remarkable total energy changes for strongly correlated electron systems (SCES) with small variation of the weight of the Hartree-Fock (HF) exchange term (our reply for the question 201). Isobe et al.<sup>15</sup> have already obtained the relative energies of possible nine intermediate under the assumption of three different weights (10%, 15% and 20 %) of the HF term. Therefore linear inter(extra)polarization procedure based on the weight ( $w$ ) of the HF term was performed to estimate the relative energies with variations of  $w$ . The energy differences between the estimated and calculated (in parentheses) values at  $w=15\%$  (UB3LYP\* by Siegbahn) are negligible, indicating that the procedure was reliable for qualitative purpose. Table S1 summarizes the relative energies for the nine intermediates in the  $S_3$  state. From Table S1, following characteristics are concluded.

- (i) The relative stability between the right (R)- and left (L\*)-opened OH-inserted structures is 9~10 kcal/mol in accord with the conclusion by Cox et al.<sup>22</sup> The left(L\*) OH<sup>-</sup> inserted structure is hardly formed at room temperature.
- (ii) The relative stability between the right (R)- and left (L)-opened OH-inserted structures is 3~4 kcal/mol in contradiction to the conclusion by Cox et al.<sup>22</sup> The left (L) OH<sup>-</sup> inserted structure is stabilized

with the hydrogen-bonding network in OEC of PSII. Therefore water exchange reaction participated with the H-bond network becomes feasible for the left (L) OH<sup>-</sup> inserted structure.

(iii) The right (R)-opened OH<sup>-</sup> inserted structure is the most stable among the nine intermediates examined under the weak correlation assumption where the weight (w) of the HF term is in the range; 0~10%. Formation of peroxo and/or superoxo species is hardly conceivable in this regime. The pure DFT such as BP86 (w=0%) and TPSSh(w=10%)<sup>22</sup> are typical DFT functionals in this regime.

(iv) The relative stability between the right (R)-opened OH<sup>-</sup> inserted and quasi-central superoxo structures becomes variable under the intermediate correlation assumption where the weight (w) of the HF term is in the range; 11~15%. The energy gaps between these structures are 5.3, 2.9, 0.2, -2.4 and -4.9 (kcal/mol), respectively, for 11, 12, 13, 14 and 15 (%) of the HF exchange (w). The superoxo structure becomes more stable than the right (R)-opened OH<sup>-</sup> inserted structure when the w-value is more than 13%.

(v) The energy gap between the right (R)-opened OH<sup>-</sup> inserted and quasi-central superoxo structures becomes large under the strong correlation assumption where the weight (w) of the HF term is in the range; 16~20%. The peroxo structure also becomes more stable than the right (R)-opened OH<sup>-</sup> inserted structure in this regime.

The relative stabilities of the nine intermediates in the S<sub>3</sub> state are sensitive to the mixing ratio of the HF exchange term, indicating that we should be very careful for discussions of the energy differences based on the HDFT computational results. For example, UB3LYP\* (w=15 %) calculation has indicated that the superoxo intermediate is more stable than the right-opened (R) hydroxide intermediate, showing that the O-O bond formation is possible in the S<sub>3</sub> state. Thus beyond HDFT computations are inevitable for quantitative discussions on possible intermediates and possible mechanisms of the water oxidation in OEC of PSII. This is our reply for the questions 200-203 and 232-234 in Faraday discussions.

(Table S1=Table 1 below).

Table 1 Relative stabilities among several intermediates in the S<sub>3</sub> state of OEC of PSII

VH DFT (W <sub>HF</sub> )	Hydroxide (OH <sup>-</sup> ,L*)	Hydroxide (OH <sup>-</sup> ,L)	OXO Mn=O (L)	OXO* Mn-O • (L)	Peroxo (L)	Superox (C)	Peroxo (R)	OXO (R)	Hydroxide (R)
0 %	9.8	4.1	4.4	16.6	27.3	33.2	25.1	6.0	0.0
5 %	9.7	3.8	4.4	14.7	18.5	20.5	17.0	3.8	0.0
8 %	9.6	3.5	4.3	13.6	13.2	12.9	12.1	2.5	0.0
10 %	9.5	3.4	4.3	12.8	9.7	7.8	8.9	1.6	0.0
12 %	9.4	3.3	4.3	12.0	6.2	2.7	5.7	0.7	0.0
15 %	9.3 (9.4)	3.1 (3.1)	4.2 (4.3)	11.2 (10.9)	1.0 (0.9)	-4.7 (-4.9)	0.9 (0.8)	-0.4 (-0.6)	0.0 (0.0)
20 %	9.2	2.7	4.2	9.0	-7.9	-17.6	-7.3	-2.8	0.0

## SIV Future prospects

### SIV.1 New SFX results for the $S_3$ state

The mechanism of water oxidation in OEC of PSII was the most important issue in our session. After the submission of this paper two SFX structures have been published for the  $S_3$  state. As mentioned above, Berkely group (Nature 540, 453-457 (2016)) proposed no water insertion in the  $S_2$  to  $S_3$  transition based on their SFX experiment. On the other hand, Okayama group (Nature 543, 131-135 (2017)) proposed water insertion in the  $S_2$  to  $S_3$  transition based on their XFEL experiment. Figure S20 illustrates schematically several proposals concerning with possible mechanisms for water oxidation in the  $S_2$  to  $S_3$  transition. Concerning with the next step of water insertion, two different scenarios have been proposed; (i) formation of the O-O bond even in the  $S_3$  state and (ii) formation of the right (R) OH<sup>-</sup> inserted structure instead of the O-O bond formation. As shown in Table S1, hybrid DFT (HDFT) level of theory is not conclusive for theoretical discrimination between the cases (i) and (ii) because of its semi-empirical nature depending on the weight (w) of the HF exchange term. Therefore HDFT computational results are often used in combination with available experimental results, for example, HDFT plus XFEL by Okayama group<sup>15</sup>, HDFT plus EPR by Cox et al<sup>22</sup>, HDFT plus EXAFS by Yale group,<sup>26</sup> etc. On the other hand, Siegbahn<sup>24</sup> is recommending the UB3LYP\* (w=15%) for theoretical prediction. We have employed the large-scale QM<sup>15</sup> and QM/MM models<sup>10,11</sup> for theoretical modeling of OEC of PSII, where the w-value is optimized so as to reproduce the post HF results for parent systems. After such calibrations, the modified HDFT is used for large systems under consideration.

### SIV.2 Importance of the system structure of OEC of PSII

Our QM/MM calculations<sup>10</sup> have elucidated the system structure of OEC of PSII in accord with the questions 203 and 204. Figure S21 illustrates through-space and through-bond pathways for water insertion in the  $S_3$  state. Here the through-space model denotes a direct water insertion into the Mn<sub>1(d)</sub> site that is five-coordinated in the  $S_2$  state of OEC of PSII. Deprotonation of the inserted water molecule at the Mn<sub>1(d)</sub> site is necessary for the through-space model. For example, Siegbahn<sup>25</sup> constructed the proton release pathway from H<sub>2</sub>O-Mn<sub>1(d)</sub> to [OH<sup>-</sup>]-Mn<sub>4(a)</sub> via putative water molecule in front of the O<sub>(5)</sub> site: Mn<sub>1(d)</sub>-H<sub>2</sub>O ... (H<sub>2</sub>O) ... [OH<sup>-</sup>]-Mn<sub>4(a)</sub>. However, such water molecule is hardly introduced in front of the O<sub>(5)</sub> site as illustrated in Fig. S22 (M. Shoji et al, Catal. Sci. Tech. 3, 1831, (2013)) because of existence of Val185 in the high-resolution XRD structure<sup>3</sup>, in contradiction to the London (Murry-Baber) model (K. N. Ferreira et al., Science 303, 1831, 2004). Thus the high-resolution XRD structure<sup>3</sup> have provided several important structural foundations for theoretical modeling of water oxidation in OEC of PSII on the basis of the QM/MM model including key aminoacid residues.<sup>10,11</sup>

The high-resolution XRD structure<sup>3</sup> have also provided the answer for a fundamental question “where are water molecules for water oxidation in OEC of PSII?”. In fact, several channels for proton transfer and water inlet pathways were elucidated on the basis of the XRD structure.<sup>3</sup> The large-scale QM/MM computations<sup>10</sup> based on the XRD structure<sup>3</sup> have also confirmed hydrogen bonding networks

which are crucial for construction of through-hydrogen bond mechanisms for water oxidation. For example, through-bond models assume a coordination of water molecule at the  $Mn_{a(4)}$  site in the initial stage of water insertion followed by shift of the inserted  $OH^-$  to the  $Mn_{1(d)}$  site as illustrated in Fig. S21. Two different pathways are proposed on the theoretical grounds based on the XRD structure<sup>3</sup>; (i) one is the shift of water molecule  $W_{11}$  coordinated to the  $O_{(4)}$  site and the other is the insertion of water molecule  $W_3$  coordinated to the  $Ca(II)$  ion. The pathways (i) and (ii) are nothing but Path III and Path II investigated by large-scale QM/MM calculations (see section SI.1).<sup>10</sup> These pathways are used for transfers of total two water molecules at each Kok cycle for water oxidation as shown in Figs. S3-S5 and S8-S9. These Figures clearly indicate the important roles of hydrogen bonding networks in OEC of PSII, namely the biomolecular system structure in accord with the questions 201-204 in Faraday discussions. The system structure will be very important for active controls of catalytic cycle of water oxidation mechanisms (see Fig. S2) with protein environments (reply for the question 203).

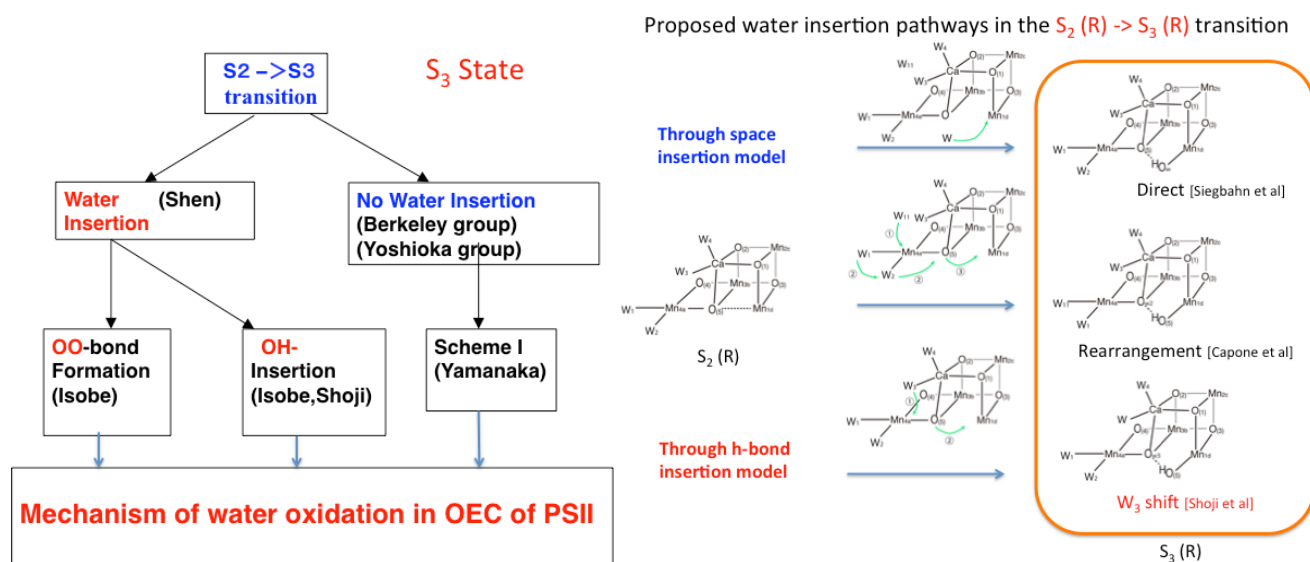


Figure S20 Water insertion the  $S_2$  to  $S_3$  transition. Figure S21 Through-space and through-bond pathways for water insertion.

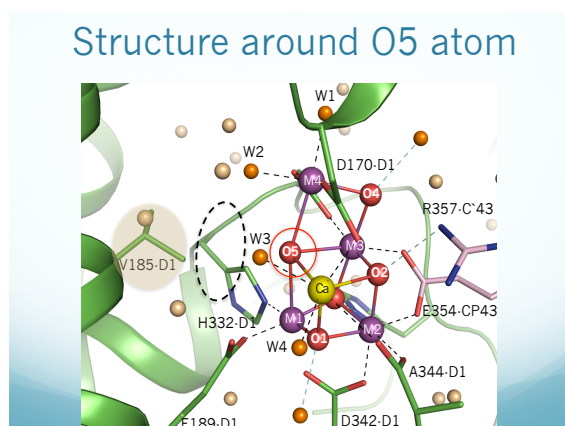


Figure S22 An important role of Val185 in front of the  $O_{(5)}$  site of OEC of PSII.

### SIV.3 Impotence of Path II and Path III for water inlet pathways

Large-scale QM/MM calculations<sup>10</sup> in Fig. 4 in the text have elucidated hydrogen-bonding networks for proton release and water inlet pathways on the basis of the high-resolution XRD structure.<sup>3</sup> From the large-scale QM/MM computational results, water molecule W10 (see Fig. S3) was linked with the nearest neighbor water molecule W20 (abbreviated): interestingly it was not fixed with aminoacid residues, showing freedom for dynamical fluctuation (see Fig. S9). Similarly, water molecule W11 (see Fig. S3) was linked with the nearest neighbor water molecule W16 (abbreviated): it was also not fixed with aminoacid residues, indicating freedom for dynamical fluctuation (see Fig. S9). This in turn means that water molecules W10 and W11 participate water oxidation within the catalytic site(s) in OEC of PSII. W20 and W16 are easily shifted to occupy the vacant sites of W10 and W14, respectively, during the water oxidation in OEC of PSII. Therefore we can assume that W10 and W14 are key molecules for water inlet pathways, Path II and Path III in our terminology<sup>10</sup>.

Kamiya et al. (J. Am. Chem. Soc. 139, 1718 (2017) ) have elucidated two subtle different structures for the A- and B-monomers, respectively, even in the  $S_1$  state of OEC of PSII by XRD, demonstrating important roles of hydrogen bonding interactions at the  $O_{(4)}$  and  $O_{(3)}$  sites of the  $\text{CaMn}_4\text{O}_5$  cluster. Suga et al also demonstrated the different hydrogen bonding interactions at the  $O_{(4)}$  site between A- and B-monomers in the  $S_3$  state. Recent experimental results indicate the necessity of theoretical investigation using realistic QM/MM models to elucidate roles of environmental conditions such as hydrogen bonding, pH, etc, for generation of different protonation structures, for example  $S_{1ab}$ ,  $S_{1ac}$  and  $S_{1bb}$  in the  $S_1$  state (see Fig. 2 in the text). This is our reply for dynamical exchange in the question 201. The QM/MM/MD simulations are now inevitable for further elucidation of dynamical mechanisms of proton transfers and water inlet in water oxidation in OEC of PSII, in complete agreement with the opinions concerning with time-dependent processes in the question 202 by Prof. Harriman.

### SIV.4 Future prospects

As shown in section SI, OEC of PSII is a complex biomolecular system (ref. 10 in the text). We have examined possible scenarios for water oxidation in OEC of PSII as shown in Scheme I and Fig. 6 in the text, and Figs. S3-S5 and S8-S9 based on the XRD structure.<sup>3</sup> Recent SFX experimental results by Arizona (Kupitz et al., Nature, 513, 261 (2014), Berkeley (Young et al., Nature 540, 453-457 (2016)) and Okayama (Suga et al, Nature 543, 131-135 (2017) groups opened the door for elucidation of true intermediates in the  $S_3$  state at room temperature. Theoretical studies on OEC of PSII are classified into three stages, (i) structure model, (ii) system model and (iii) dynamical model, in conformity with developments of various experimental studies as illustrated in Fig. S22. Many QM models have been proposed for the step (i) for elucidation of four degrees of freedom of the  $\text{CaMn}_4\text{O}_5$  cluster in Fig. S3. Several QM/MM models are also proposed for the second step (ii) for theoretical investigations of biomolecular system structures of OEC of PSII, namely the question 201 in Faraday discussion. QM/MM/MD simulations are crucial for elucidation of dynamical (catalytic cycles) mechanisms for

water oxidation in OEC of PSII, namely the question 202 in Faraday discussion. Cooperative efforts of experimental and theoretical approaches to OEC of PSII are expected to elucidate the mechanism of water oxidation using sunlight (question 203), namely energy conversion of light energy into chemical energy. A theoretical movie for such processes by a post Kei computer is our dream in future.

Theoretical investigation of the native OEC of PSII provides a bio-inspired guiding principle for construction of artificial photosynthetic systems. Figure S13 illustrates our theoretical view of the  $\text{CaMn}_4\text{O}_5$  cluster in OEC of PSII, namely strongly correlated electron system (SCES) confined with protein. The SECS core in OEC of PSII can be replaced with other several 3d metals complexes with robust coordination ligands and protein is replaced with other confinement materials in artificial photosynthesis (AP) as illustrated in Fig. S13. Several 3d metals such as Fe, Cu, etc are abundant metals in our Earth. Design of antenna systems for light harvesting is also important for developments of AP systems (the question 202).

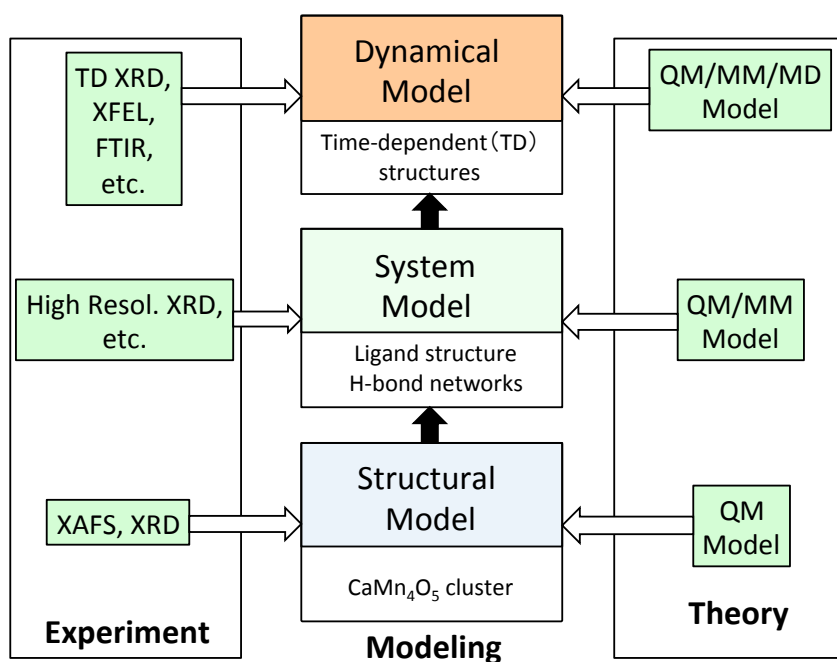


Fig. S23 Three theoretical models for elucidation of water oxidation in OEC of PSII in cooperative efforts with various experimental investigations. Similar approaches are also feasible for theoretical investigations of artificial devices for water oxidation.